electrodes were sectioned to eliminate afferent signals from the heart. To insulate and fix the electrodes, the nerves and electrodes were secured with silicone glue (Kwik-Sil, World Precision Instruments, Sarasota, FL). The preamplified nerve signals were band-pass filtered at 150–1,000 Hz, full-wave rectified, and low-pass filtered at a cutoff frequency of 30 Hz by using analog circuit. After that, the neural signals were recorded at a sampling rate of 200 Hz using a 12-bit analog-to-digital converter. Pancuronium bromide (0.1 mg/kg) was administered to prevent contaminating muscular activities. At the end of the experiment, the experimental animals were killed by an overdose of intravenous pentobarbital sodium, and the background noise level of SNA was determined postmortem.

Sixteen of the 22 rabbits were used in *protocol 1 (protocols 1-1, 1-2, and 1-3)*, and the remaining 6 rabbits were used in *protocols 2, 3,* and *4*. In 10 of the 16 rabbits for *protocols 1-2* and/or *1-3* described below, we isolated both carotid sinuses from the systemic circulation by ligating the internal and external carotid arteries and other small branches originating from the carotid sinus regions. The isolated carotid sinuses were filled with warmed physiological saline through catheters inserted via the common carotid arteries. The intra-carotid sinus pressure (CSP) was controlled by a servo-controlled piston pump (model ET-126A, Labworks, Costa Mesa, CA). In the baroreflex open-loop experimental settings, bilateral vagal and aortic depressor nerves were sectioned at the neck to minimize reflex effects from cardiopulmonary regions and the aortic arch.

Electroacupuncture

Two stainless steel needles were inserted at the one-fifth point (from the knee) and the midpoint of the knee-ankle distance of approximately 30–35 mm. These needles with a diameter of 0.2 mm (CE0123, Seirin-Kasei, Shimizu City, Japan) were inserted to a depth of ~10 mm in the skin and underlying muscle (the right tibialis anterior muscle). This area corresponds to the Zusanli and Xiajuxu acupoints (over the peroneal nerve below the knee, stomach meridian, St 36 and 39) in humans.

As in previous studies (2, 3, 17, 42), the stimulus current intensity was determined as 10 times of twitch threshold, which is the minimal electrical current required for eliciting visible muscle twitches of the stimulated leg. Actually, the current was 4.8 ± 0.3 mA (4.2–5.4 mA). An electric rectangular wave current with a frequency of 1 Hz and with pulse duration of 5 ms was passed between these two needles by using an electrical stimulator (SEN-7203, Nihon Kohden) except *protocol 4* where shorter pulse durations were challenged.

Protocols

The experimental protocol was approved by the Animal Experimental Committee of National Cardiovascular Center Research Institute.

Protocol 1: effect of Zusanli electroacupuncture on AP, SNA, and baroreflex. PROTOCOL 1-1 (BAROREFLEX CLOSED-LOOP CONDITION, N = 6). To elucidate the overall cardiovascular inhibitory effects of electroacupuncture, we performed 1 Hz electroacupuncture for 8 min and measured AP and SNA responses under conditions of intact cardiovascular reflexes. In this closed-loop protocol, vagal and aortic depressor nerves were preserved. Baseline data were measured for 1 min before acupuncture insertion. At 10 min after acupuncture insertion, baseline data were measured again for 1 min. Electroacupuncture was applied for 8 min. The recovery data were measured for 2 min after the cessation of electroacupuncture.

PROTOCOL 1-2 (BAROREFLEX OPEN-LOOP CONDITION, N = 8). To elucidate the effects of electroacupuncture on the arterial baroreflex over an entire operating range, we performed a baroreflex open-loop experiment as follows. CSP was first decreased to 40 mmHg. After attainment of a steady state, CSP was increased from 40 to 160 mmHg in increments of 20 mmHg. Each pressure step was maintained for 60 s. We measured AP and SNA during the stepwise increase in CSP. Two trials (control and electroacupuncture trials) were performed on

each rabbit. The order of the trials was randomized. The electroacupuncture trial was identical to the control trial except that electroacupuncture was commenced 1 min before the initiation of stepwise increase in CSP.

PROTOCOL 1-3 (BAROREFLEX OPEN-LOOP CONDITION WITH PERONEAL DENERVATION, N = 6). To identify the afferent pathway of electroacupuncture, we examined the effects of 1 Hz electroacupuncture on the arterial baroreflex after severing the right peroneal nerve at the level of the knee joint. Estimation of the baroreflex equilibrium diagram was conducted as in *protocol 1-2* in the control and electroacupuncture trials. Four of the six rabbits had also undergone *protocol 1-2*.

Protocol 2: effects of sham (nonelectrical) acupuncture at Zusanli and control (nonspecific) electrical and nonelectrical acupunctures on AP and SNA in baroreflex closed-loop condition (n = 6). To determine whether changes in AP and SNA during Zusanli electroacupuncture are specific responses, sham and control acupunctures were conducted under the following acupuncture conditions: *1*) no acupuncture (nonacupuncture), *2*) nonelectrical acupuncture at Zusanli-Xiajuxu (St 36–39) acupoints (sham acupuncture), *3*) nonelectrical acupuncture at Guangming-Xuanzhong (gallbladder meridian, Gb 37–39) acupoints (control acupuncture), and *4*) electrical acupuncture at Guangming-Xuanzhong acupoints (control electroacupuncture). We chose Guangming-Xuanzhong as nonspecific control acupoints (*trials 3* and *4*) because these acupoints are believed to reduce leg pain without affecting the cardiovascular system, in contrast to the Zusanli-Xiajuxu acupoints. In each trial, AP and SNA were measured for a baseline duration of 1 min, under acupuncture condition (*trial 1, 2, 3,* or *4*) for 8 min, and recovery for 1 min.

Protocol 3: effect of long-term Zusanli electroacupuncture on AP and SNA in baroreflex closed-loop condition (n = 6). To clarify the effect of long-term electroacupuncture on cardiovascular system, AP and SNA were measured during and after 30 min of electroacupuncture at Zusanli-Xiajuxu acupoints. *Protocol 3* was conducted in the same manner as *protocol 1-1* except with a longer stimulation duration than *protocol 1-1* (8 min).

Protocol 4: Effect of pulse duration of Zusanli electroacupuncture on AP and SNA in baroreflex closed-loop condition (n = 6). To examine the effect of pulse duration of electroacupuncture on AP and SNA, AP and SNA were measured during electroacupuncture at Zusanli-Xiajuxu acupoints with the pulse duration increasing stepwise from 0.1 to 0.25, 0.5, 1, 2.5, 5, and 10 ms, every 60 s. In each animal, the frequency and stimulus current intensity were maintained constant as in *protocols 1, 2,* and *3*.

Data Analysis

We recorded CSP, SNA, and AP at a sampling rate of 200 Hz by using a 12-bit analog-to-digital converter. Data were stored on the hard drive of a dedicated laboratory computer system for later analyses.

In *protocol 1-1, 2, and 4*, mean AP and SNA for 1 min were calculated for baseline conditions, every minute of electroacupuncture, and recovery. In *protocol 3*, mean AP and SNA for 5 min were calculated for baseline conditions, electroacupuncture, and recovery. In *protocols 1-2* and *1-3*, we calculated mean AP and SNA during the last 10 s of each CSP step. Because the absolute magnitude of SNA depended on recording conditions, SNA was presented in arbitrary units (au). The background noise level was set at 0 au and the SNA value at the closed-loop operating point in the control trial (without electroacupuncture) was set at 100 au for each animal.

A four-parameter logistic function analysis was performed on the neural arc (CSP-SNA data pairs) and the peripheral arc (SNA-AP data pairs) as follows (11)

$$y = \frac{P_1}{1 + \exp[P_2(x - P_3)]} + P_4 \qquad (1)$$

where x and y represent the input and the output, respectively. P_1 denotes the response range (i.e., the difference between the maximum and minimum values of y), P_2 is the coefficient of gain, P_3 is the midpoint of the logistic function on the input axis, and P_4 is the minimum value of y. The maximum gain (G_{max}) is calculated from $-P_1P_2/4$ at $x = P_3$. The parameter values were calculated by an iterative nonlinear least-squares regression known as the downhill simplex method.

Statistical Analysis

All data are presented as means $\pm$ SD. Differences were considered to be significant when $P < 0.05$. In *protocols 1-1, 2, 3,* and *4,* the effects of electroacupuncture on AP and SNA at different time intervals were evaluated by one-way ANOVA. The Dunnett's test was used for multiple comparisons. In *protocols 1-2* and *1-3,* the effects of electroacupuncture on the four parameters of the logistic functions relating to the neural and peripheral arcs, as well as on the closed-loop operating point, were examined by using a paired t-test.

RESULTS

Figure 1A (*protocol 1-1*) shows a typical time series of AP and SNA in response to Zusanli-Xiajuxu electroacupuncture with intact cardiovascular reflexes. AP and SNA were reduced immediately after beginning electroacupuncture, and these remained reduced during 8-min electroacupuncture. Figure 1B illustrates the group-averaged AP and SNA in response to electroacupuncture. AP and SNA for baseline were unchanged by acupuncture insertion alone, while these values for 8-min electroacupuncture remained decreased from baseline. These values returned to baseline level after the cessation of electroacupuncture.

Figure 2 (*protocol 1-2*) shows a typical AP and SNA response to the increments in CSP in the control (Fig. 2, *left*) and electroacupuncture (Fig. 2, *right*) trials. A stepwise increase in CSP decreased SNA and AP in both trials. In the electroacupuncture trial, the AP and SNA response ranges to CSP were attenuated compared with the control trial.

Figure 3, *A* and *B* (*protocol 1-2*), shows the averaged baroreflex neural and peripheral arcs obtained in control and electroacupuncture trials. The neural arc showed a sigmoidal relationship between CSP and SNA. In the neural arc, the response range of SNA (P_1) and midpoint of the operating
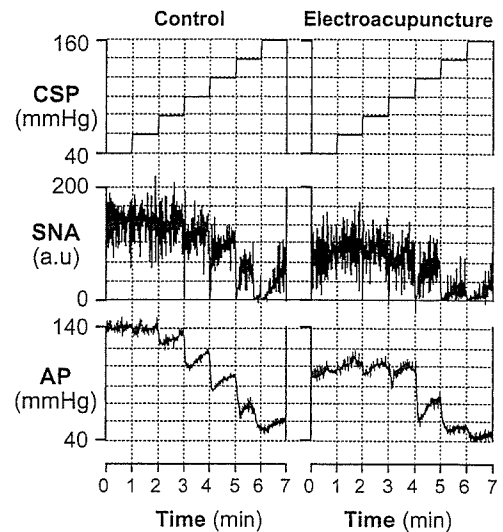

Fig. 2. Typical time series of intra-carotid sinus pressure (CSP), AP, and SNA in control (*left*) and electroacupuncture trials (*right*) in *protocol 1-2*. SNA and AP decreased in response to increments in CSP in both of the two trials. The response ranges of AP and SNA to CSP were lower in electroacupuncture than in controls.

range (P_3) were significantly decreased by electroacupuncture (Table 1). The coefficient of gain (P_2), the minimum value of SNA (P_4), and G_{max} did not differ between the two trials (Table 1). As a result, the maximum value of SNA, calculated from $P_1 + P_4$, was significantly decreased by electroacupuncture from 162 ± 31 to 130 ± 29 au ($P < 0.005$). The peripheral arc showed a more linear relationship between SNA and AP than the neural arc. In the peripheral arc, electroacupuncture did not affect any of the four parameters or G_{max} (Table 1 and Fig. 3B). The operating point determined by the intersection of the neural and peripheral arcs was moved toward lower AP and SNA (from *point a* to *point b*) by electroacupuncture (Fig. 3C and Table 1).

Figure 4 (*protocol 1-3*) shows the averaged baroreflex neural (Fig. 4A) and peripheral arcs (Fig. 4B) in control and electroacupuncture trials with severance of the peroneal nerve innervating the tibialis anterior muscle. Two arcs obtained in both trials were nearly superimposable. The four parameters and G_{max} in the neural and peripheral arcs and operating point were

Fig. 1. Typical time series of arterial pressure (AP) and sympathetic nerve activity (SNA) during 8 min of 1-Hz electroacupuncture (*A*) and the averaged ($n = 6$) AP and SNA (*B*) in *protocol 1-1*. Data include periods of baseline (Base, 1 min), electroacupuncture (8 min), and recovery (Rec, 1 min). Each data point represents average values over 1 min. #*P* < 0.05: significantly different from baseline after acupuncture insertion. au, Arbitrary units.
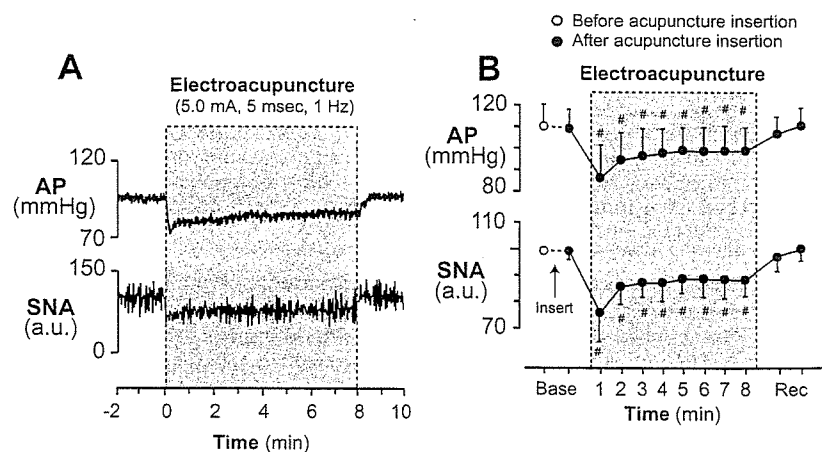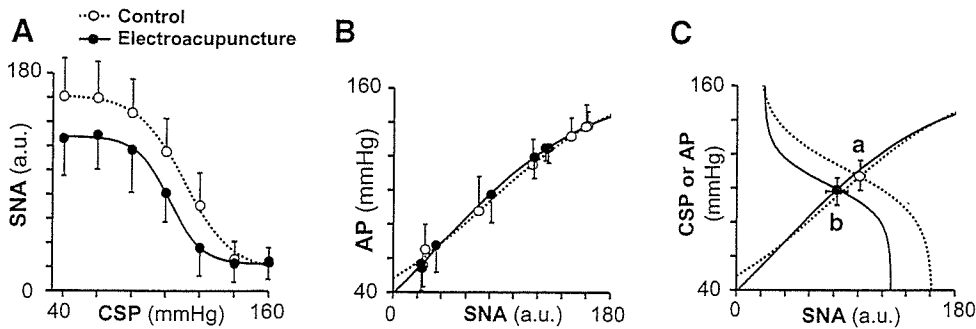
Fig. 3. Averaged ($n = 8$) baroreflex neural arc (A), peripheral arc (B), and baroreflex equilibrium diagram (C) obtained in 8 rabbits in control (O) and electroacupuncture (●) trials in protocol 1-2. Electroacupuncture shifted the neural arc to lower SNA (A), but it did not change the peripheral arc (B). The shift in neural arc reduced AP and SNA by 9 ± 3 mmHg and 20 ± 10 au (from point a to point b) at the operating point (C).

not affected by electroacupuncture when the peroneal nerve was denervated (Table 2 and Fig. 4C).

Figure 5 (protocol 2) shows the changes in AP and SNA during nonacupuncture (without acupuncture), sham acupuncture [nonelectrical acupuncture at Zusanli-Xiajuxu (St 36–39)], control acupuncture [nonelectrical acupuncture at Guangming-Xuanzhong (Gb 37–39)] and control electroacupuncture (electrical acupuncture at Gb 37–39) trials. AP and SNA did not change in these trials.

Figure 6, A and B (protocol 3), shows a typical time series and the averaged data, respectively, of AP and SNA in response to long-term Zusanli-Xiajuxu electroacupuncture. AP and SNA decreased immediately after electroacupuncture was started and remained reduced during 30-min electroacupuncture. In addition, AP and SNA returned to the preelectroacupuncture baseline levels immediately after cessation of electroacupuncture.

Figure 7, A and B (protocol 4), shows a typical time series and the averaged data, respectively, of AP and SNA during Zusanli-Xiajuxu electroacupuncture with the pulse duration increasing from 0.1 to 5 ms. Although increasing the pulse duration from 0.1 to 1 ms did not change AP and SNA, pulse durations of 2.5 ms and higher decreased SNA while pulse durations of 5 and 10 ms decreased AP.

Table 1. Effect of electroacupuncture on the operating point of baroreflex and on the 4 parameters of logistic functions approximating neural and peripheral baroreflex arcs

	Control	Electroacupuncture
Operating point		
Arterial pressure, mmHg	108.4±8.7	98.8±7.9†
Sympathetic nerve activity, au	99.8±4.1	80.0±8.9†
Neural arc		
P_1, au	144.0±35.0	112.6±9.2†
P_2, au/mmHg	0.08±0.03	0.09±0.09
P_3, mmHg	111.4±6.5	103.3±10.0*
P_4, au	17.5±6.1	17.4±8.7
G_{max}, au/mmHg	−2.94±0.91	−2.58±1.27
Peripheral arc		
P_1, mmHg	129.6±20.5	125.9±19.5
P_2, au/mmHg	−0.03±0.01	−0.03±0.01
P_3, au	80.6±23.2	71.7±17.1
P_4, mmHg	29.9±16.3	29.5±12.1
G_{max}, mmHg/au	0.74±0.10	0.84±0.18

Values are means ± SD ($n = 8$). G_{max}, maximum gain. See Data Analysis for definition of 4 parameters of logistic function. au, Arbitrary units. *$P <$ 0.05 and †$P <$ 0.005 vs. control.

DISCUSSION

The major new finding of the present study was that electroacupuncture at Zusanli resets the arterial baroreflex neural arc to lower SNA but does not significantly affect the baroreflex peripheral arc. As a result, the operating point determined by the intersection of the neural and peripheral arcs was moved toward lower SNA and AP by electroacupuncture. To the best of our knowledge, this is the first study delineating the effects of short-term electroacupuncture on the arterial baroreflex over an entire operating range.

Effects of Electroacupuncture on the Arterial Baroreflex (Protocol 1)

The arterial baroreflex system is one of the most important negative-feedback systems that stabilize AP against exogenous disturbances. When AP is decreased by exogenous perturbation such as blood loss, the reduction in AP is sensed by the arterial baroreceptors. SNA is then increased by the arterial baroreflex to buffer the reduction in AP. In such circumstances, SNA and AP change reciprocally. On the other hand, when SNA is changed by an exogenous perturbation such as emotional stress, SNA and AP change in parallel. In protocol 1-1, electroacupuncture decreased both SNA and AP, indicating that electroacupuncture introduced exogenous perturbation to decrease SNA with a resultant reduction in AP. Although the net effect of electroacupuncture is to decrease SNA, the perturbation of AP cannot be excluded. For example, because electroacupuncture also twitched the hindlimb muscles, electroacupuncture might have perturbed AP via changes in vascular resistance and/or venous return through muscle pump function. Therefore, to quantify the contribution of both perturbations on SNA and on AP, we performed protocol 1-2. Perturbation of AP is most easily detected by comparing AP at the same SNA level with and without electroacupuncture.

In protocol 1-2, we performed a baroreflex open-loop experiment and identified the static characteristics of the neural and peripheral arcs over a wide operating range. As expected, electroacupuncture shifted the neural arc toward lower SNA and decreased maximum SNA to ~80% of control (Fig. 3A). This shift is not due to reduced perfusion to the medulla by AP reduction during electroacupuncture because the AP was decreased by ~10 mmHg and would not induce cerebral ischemia. In contrast, electroacupuncture had little effect on the peripheral arc (Fig. 3B). In other words, AP with and without electroacupuncture did not differ significantly at any of the SNA levels. Therefore, changes in AP observed in protocol 1-1
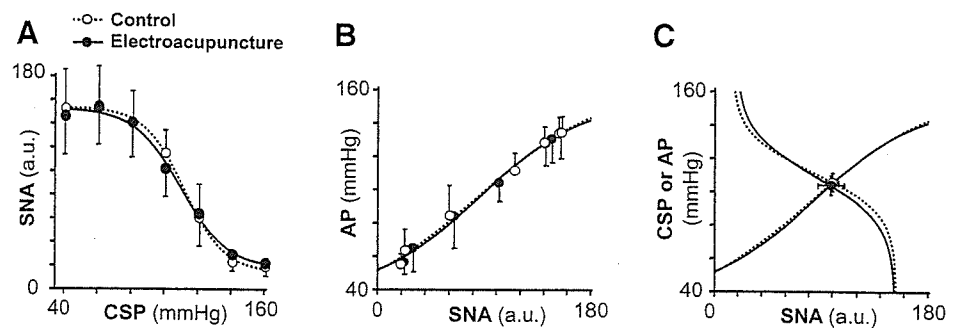
Fig. 4. Averaged ($n = 6$) baroreflex neural arc (A), peripheral arc (B), and baroreflex equilibrium diagrams (C) obtained in 6 rabbits in control (○) and electroacupuncture (●) trials with peroneal denervation in *protocol 1-3*. The baroreflex neural arc, peripheral arc, and the operating point were not influenced by electroacupuncture after peroneal denervation.

were attributable exclusively to perturbation of SNA and not to possible perturbation effects of electroacupuncture on AP.

The neural and peripheral arcs were combined to yield a baroreflex equilibrium diagram (Fig. 3C). The closed-loop operating point, determined by the intersection of the neural and peripheral arcs, moved from *point a* to *point b* during electroacupuncture. Despite a significant shift in the closed-loop operating point, neither the neural nor peripheral arc gain was altered significantly (Table 1). The fact that the baroreflex gain was maintained during electroacupuncture suggests the possible application of electroacupuncture to the treatment of cardiovascular diseases with sympathetic hyperactivity. However, the preservation of the arterial baroreflex gain in the present experimental settings may rely on normal peripheral arc characteristics. Cardiovascular diseases such as heart failure may decrease the peripheral arc gain to a variable extent due to impaired pump function. Whether the arterial baroreflex function during electroacupuncture can be maintained in cardiovascular diseases awaits future study.

Mechanisms for the Cardiovascular Inhibitory Effects of Electroacupuncture (Protocol 1)

The resetting in the baroreflex neural arc during electroacupuncture was mediated by a somatosympathetic reflex arising from the stimulated hindlimb, as evidenced by the fact that

peroneal denervation abolished the resetting (Table 2 and Fig. 4). This result was consistent with an earlier study (27) showing that depressor and sympathoinhibitory responses during acupuncture were abolished by sciatic and femoral denervation. The existence of a somatosympathetic reflex is also supported by the fact that electrical stimulation of somatic afferents reduced AP (7–9). Legramante et al. (14) showed that rapidly conducting group III somatic afferent activation can evoke AP reduction during 1-Hz electrical stimulation of the tibial nerve. In contrast, high-frequency stimulation of the somatic afferent evokes AP elevation. Passive muscle stretching, which is considered to activate group III somatic afferent fibers, shifts the baroreflex neural arc toward higher SNA, resulting in an increase in the closed-loop operating point (41). The mechanism of two opposing influences of somatic afferent activation depending on the stimulation frequency is not fully understood.

Table 2. *Effect of electroacupuncture with peroneal denervation on the operating point of baroreflex and on the 4 parameters of logistic functions approximating neural and peripheral baroreflex arcs*

	Control	Electroacupuncture
Operating point		
Arterial pressure, mmHg	105.7±5.7	104.1±5.6
Sympathetic nerve activity, au	99.8±5.1	98.3±11.1
Neural arc		
P_1, au	138.3±42.4	136.3±38.6
P_2, au/mmHg	0.11±0.03	0.08±0.03
P_3, mmHg	112.7±10.2	111.5±10.6
P_4, au	14.9±8.7	15.7±7.4
G_{max}, au/mmHg	−3.27±1.15	−2.84±1.12
Peripheral arc		
P_1, mmHg	144.1±35.5	140.5±34.4
P_2, au/mmHg	−0.02±0.002	−0.02±0.004
P_3, au	82.0±34.0	78.8±32.0
P_4, mmHg	26.1±8.1	25.5±5.3
G_{max}, mmHg/au	0.69±0.13	0.72±0.21

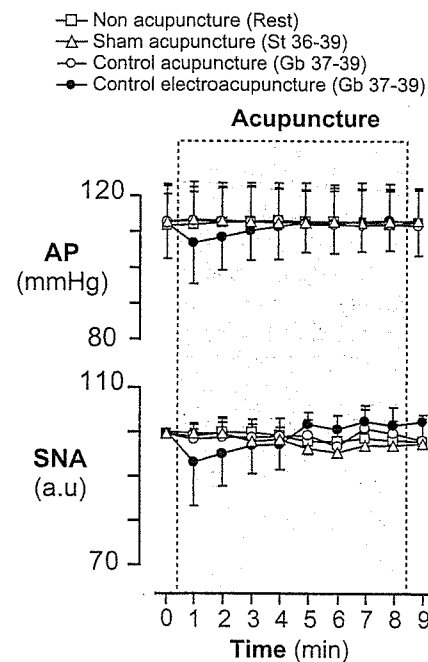Values are means ± SD ($n = 6$). See *Data Analysis* for definition of 4 parameters of logistic function.

Fig. 5. Averaged ($n = 6$) AP (*top*) and SNA (*bottom*) in nonacupuncture (condition without acupuncture, □), sham acupuncture [nonelectrical acupuncture at Zusanli-Xiajuxu (stomach meridian, St 36–39), △], control acupuncture [nonelectrical and acupuncture at Guangming-Xuanzhong (gallbladder meridien, Gb 37–39), ○], and control electroacupuncture [electrical acupuncture at Gb 37–39, ●] trials in *protocol 2*. Data include periods of baseline (1 min), electroacupuncture (8 min), and recovery (1 min). Each data point represents average values over 1 min.
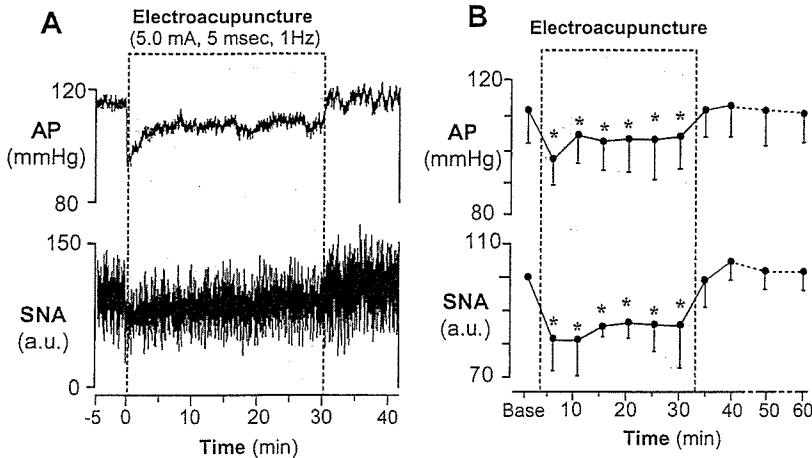
Fig. 6. Typical time series of AP and SNA during 30 min of 1-Hz electroacupuncture (St 36–39; *A*) and the averaged (*n* = 6) AP and SNA (*B*) in *protocol 3*. Data include periods of baseline (5 min), electroacupuncture (30 min), and recovery (30 min). Each data point represents averaged values over 5 min during baseline, electroacupuncture, and the first 10 min of recovery and those over 10 min during the last 20 min of recovery. *$P < 0.05$: significantly different from baseline after acupuncture insertion.

Another explanation for resetting in the neural arc may be circulatory endogenous opioids (e.g., β-endorphin and enkephalin), which are released from the adrenal gland and hypothalamus by prolonged (>30 min) electroacupuncture (20, 21). These endogenous opioids are known to modulate the arterial baroreflex (24, 29, 35). However, changes in endogenous opioids are unlikely to be the mechanism for reductions in SNA and AP by electroacupuncture in the present experimental settings because the inhibitory effects terminated immediately after cessation of electroacupuncture rather than lasting for several hours (42) (Fig. 1).

Previous studies suggest a central interaction between an electroacupuncture-evoked somatosympathetic reflex and the arterial baroreflex. Baroreceptor afferent inputs inhibit neural activities in the rostral ventrolateral medulla (rVLM) (6, 33). Tjen-A-Looi et al. (36) showed that electroacupuncture inhibited rVLM neural activities, suggesting that the electroacupuncture-evoked somatosympathetic reflex and arterial baroreflex share common central pathways. In addition, 2-Hz electroacupuncture inhibits SNA through the excitation of β-endorphinergic and GABAergic neurons to rVLM (12, 13).

Central interaction in the brain stem may be involved in the resetting of the arterial baroreflex neural arc induced by electroacupuncture.

Characteristics of Zusanli-Xiajuxu Electroacupuncture Used in the Present Study

The Zusanli electroacupuncture used in this study has some unique characteristics. First, our results showed that baseline AP and SNA were decreased significantly by electroacupuncture, in contrast to previous studies that found no significant reduction in baseline AP and SNA during Zusanli electroacupuncture in rats (0.5-ms duration, 1–2 mA, 2 Hz) (18) and nonelectrical acupuncture in normotensive humans (right large intestine 4, right liver 3, and left spleen 6) (22). Second, our result showed that AP and SNA were reduced as soon as electroacupuncture was started, in contrast to previous reports that the effect of Zusanli electroacupuncture did not even begin to manifest for the first 10–15 min in rats (0.5-ms duration, 1–2 mA, 2 Hz) (18) and cats (0.5-ms duration, 0.4–0.6 mA, 2–4 Hz) (37). These discrepancies may be related to the differences in acupoints and stimulation conditions (pulse duration, current, and frequency). In particular, the pulse duration used in our study (5 ms) was approximately 10–50 times longer than that used in previous studies. Indeed, the data obtained from *protocol 4* show that increasing the pulse duration augments the reduction in AP and SNA during electroacupuncture; pulse durations shorter than 2.5 ms did not change AP and SNA, whereas durations of 2.5 ms and above decreased both parameters immediately after the electroacupuncture was started (Fig. 7). In addition, our data suggest that stimulation duration (<2.5 ms) does not affect arterial baroreflex, consistent with our preliminary data that baroreflex neural, peripheral, and total arcs remained unchanged during electroacupuncture with pulse durations <2.5 ms (unpublished data). These observations may indicate that the effect of electroacupuncture on arterial baroreflex is linked to the stimulation pulse duration.

The third characteristic is that the inhibitory effects of electroacupuncture on AP and SNA disappeared immediately after the cessation of electroacupuncture. In contrast, some studies showed that the inhibitory effects of electroacupuncture on AP lasted for 10–60 min after the cessation (18). The characteristics in this study may not be explained by the length of electroacupuncture because AP and SNA recovered to the
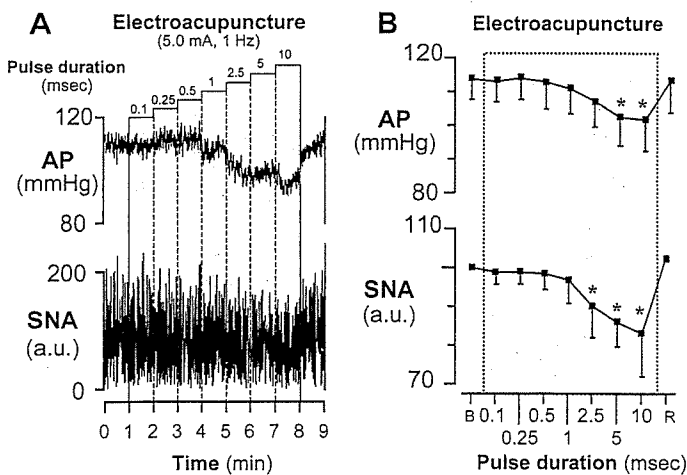

Fig. 7. Typical time series of AP and SNA during 1-Hz electroacupuncture with increasing the pulse duration (*A*) and the averaged (*n* = 6) AP and SNA (*B*) in *protocol 4*. Data include periods of baseline (B, 1 min), electroacupuncture (7 min), and recovery (R, 1 min). Each data point represents average values over 1 min. *$P < 0.05$; significantly different from baseline after acupuncture insertion.
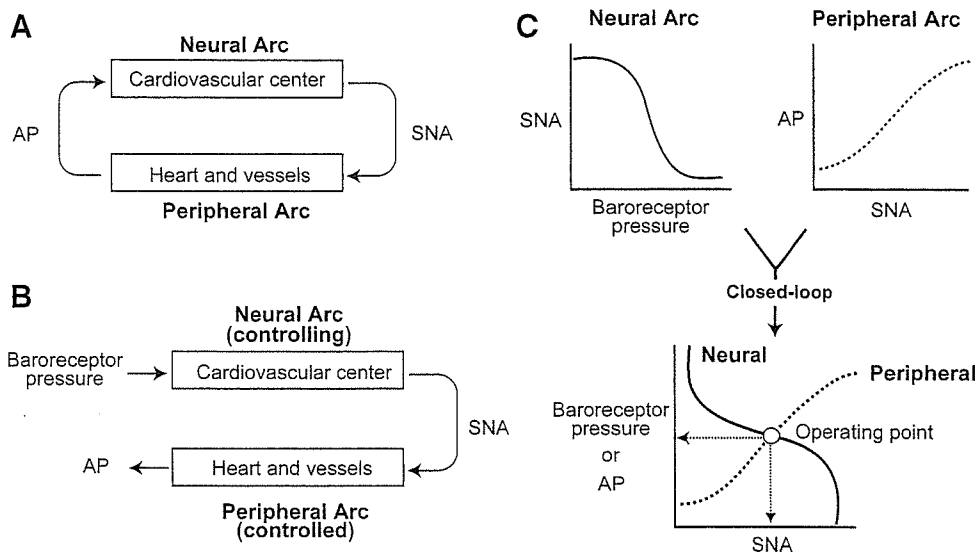
Fig. 8. Arterial baroreflex system in closed-loop (A) and open-loop (B) conditions. In open-loop conditions, the relationships between baroreceptor pressure and SNA (the neural arc) and between SNA and AP (the peripheral arc) can be quantitatively measured. Intersection of the neural and peripheral arcs corresponds to the operating point of AP and SNA under closed-loop conditions of feedback (C).

prestimulation baseline levels immediately after the cessation in both short-duration (8 min, Fig. 1) and longer-duration electroacupuncture (30 min, Fig. 6) protocols. The rapid disappearance of effects suggests that the AP and SNA reductions seen in the present study may not be elicited by the opioid mechanism, although clinical experiments with longer-duration electroacupuncture have demonstrated long-lasting effects on the cardiovascular system, which are attributed to opioid substances (2, 12, 15, 37, 42).

The reductions in AP and SNA during Zusanli electroacupuncture seen in the present study may not be just a nonspecific response to acupunctures. Our data from *protocol 2* (Fig. 5) showed that nonelectrical acupuncture at Zusanli (sham acupuncture) did not decrease AP and SNA, suggesting that the AP and SNA reductions during Zusanli electroacupuncture are not simply the results from insertion of acupuncture needles. Furthermore, acupuncture at Guangming-Xuanzhong (control acupuncture, control electroacupuncture) did not change AP and SNA regardless of electrical stimulation (Fig. 5). This result suggests the importance of acupoint specificity and is consistent with an earlier study showing point-specific differences in cardiovascular inhibitory responses (Jiangshi-Neiguan or Shousanli-Quchi acupoints vs. Pianli-Wenlui or Zusanli-Shangjuxu acupoints) (37). These observations may support the concept that Zusanli acupuncture changes cardiovascular variables in experimental animal models (4, 25, 28) and confers beneficial effects on cardiovascular diseases (5, 30, 34), whereas Guangming-Xuanzhong acupuncture does not affect cardiovascular variables (18).

Limitations

There are several limitations to this study. First, as anesthesia affects the autonomic nervous system, the results might have been different without anesthesia. Second, our isolation of the carotid sinus regions may stimulate carotid chemoreceptors. However, in determining baroreflex function, this factor was present in trials with and without electroacupuncture. Therefore, we believe that this factor may not affect our conclusion of baroreflex resetting during electroacupuncture.

Third, acupuncture was inserted at a point corresponding to the Zusanli acupoint in humans. When acupuncture is properly

inserted at the acupoint, the patient feels heaviness or soreness. Such sensory information is not available in an anesthetized animal. Because electroacupuncture (as distinct from acupuncture with no electrical stimulation) stimulates not only the inserted point but also the surrounding area, it has been used as a convenient way of stimulating acupoints in patients and in experimental animals. Thus, even if we failed to insert the needle at the precise acupoint, we believe that Zusanli could be stimulated electrically.

Fourth, although we determined the effects of electroacupuncture at Zusanli acupoints on cardiovascular and baroreflex systems, there are other important acupoints that are able to influence these systems. In particular, Neiguan electroacupuncture is actually known to decrease sympathetic premotor neuron activity for a longer period than Zusanli electroacupuncture (36, 37). Further studies are necessary to determine the effect of Neiguan electroacupuncture on the arterial baroreflex.

Last, we evaluated the effects of Zusanli electroacupuncture on the baroreflex function for a short acupuncture duration of only 8 min. Because electroacupuncture is typically practiced for longer periods of time, our results have limited applicability. However, the electroacupuncture we used decreased AP and SNA immediately after application, showing that the procedure has acute effect on the cardiovascular system. That was the reason why we focused on the effect of short duration electroacupuncture on the baroreflex system. Future study is necessary to examine the effects of longer-duration electroacupuncture.

In conclusion, 1 Hz, short-term electroacupuncture of Zusanli reset the baroreflex neural arc toward lower SNA but did not affect the peripheral arc. The closed-loop operating point determined by the intersection of the neural and peripheral arcs was moved toward lower SNA and AP by electroacupuncture.

APPENDIX

Theoretical Considerations: Coupling of Neural and Peripheral Arcs

Changes in AP are immediately sensed by arterial baroreceptors, which alter efferent SNA via the cardiovascular center of baroreflex (Fig. 8A). Efferent SNA in turn governs heart rate and the mechanical

properties of the heart and vessels, which themselves exert a direct influence over AP. This negative-feedback loop makes it difficult to analyze the behavior of the arterial baroreflex. To overcome this problem, we opened the negative-feedback loop and divided the system into controlling and controlled elements (31). We defined the controlling element as the neural arc and the controlled element as the peripheral arc (Fig. 8B). In the neural arc, the input is the pressure sensed by the arterial baroreceptors and the output is SNA. In the peripheral arc, the input is SNA and the output is AP (Fig. 8C). Because pressure sensed by the arterial baroreceptor is equilibrated with AP under physiological conditions, we superimposed the functions of the two arcs and determined the operating point of the system from the intersection of the two arcs. The operating point is defined as the AP and SNA under closed-loop conditions of the feedback system. The validity of this framework has been examined in previous studies (10, 31). Using the baroreflex equilibrium diagram, we aimed to quantify the effects of electroacupuncture on the arterial baroreflex.

GRANTS

REFERENCES

1. **Brickman AL, Calaresu FR, and Mogenson GJ.** Bradycardia during stimulation of the septum and somatic afferents in the rabbit. *Am J Physiol Regul Integr Comp Physiol* 236: R225–R230, 1979.

2. **Chao DM, Shen LL, Tjen-A-Looi S, Pitsillides KF, Li P, and Longhurst JC.** Naloxone reverses inhibitory effect of electroacupuncture on sympathetic cardiovascular reflex responses. *Am J Physiol Heart Circ Physiol* 276: H2127–H2134, 1999.

3. **Chen S and Ma SX.** Nitric oxide in the gracile nucleus mediates depressor response to acupuncture (ST36). *J Neurophysiol* 90: 780–785, 2003.

4. **Chiu DTJ and Cheng KK.** A study of the mechanism of the hypotensive effect of acupuncture in the rat. *Am J Chin Med* 2: 413–419, 1974.

5. **Chiu YJ, Chi A, and Reid IA.** Cardiovascular and endocrine effects of acupuncture in hypertensive patients. *Clin Exp Hypertens* 19: 1047–1063, 1997.

6. **Dampney RA, Horiuchi J, Tagawa T, Fontes MA, Potts PD, and Polson JW.** Medullary and supramedullary mechanisms regulating sympathetic vasomotor tone. *Acta Physiol Scand* 177: 209–218, 2003.

7. **Johansson B.** Studies on cardiovascular responses induced by electrical stimulation of afferent somatic nerves. A preliminary report. *Med Exp Int J Exp Med* 5: 447–453, 1961.

8. **Johansson B.** Circulatory responses to stimulation of somatic afferents with special reference to depressor effects from muscle nerves. *Acta Physiol Scand Suppl* 198: 1–91, 1962.

9. **Johansson B, Lundgren O, and Mellander S.** Reflex influence of "somatic pressor and depressor afferents" on resistance and capacitance vessels and on transcapillary fluid exchange. *Acta Physiol Scand* 62: 280–286, 1964.

10. **Kawada T, Shishido T, Inagaki M, Zheng C, Yanagiya Y, Uemura K, Sugimachi M, and Sunagawa K.** Estimation of baroreflex gain using a baroreflex equilibrium diagram. *Jpn J Physiol* 52: 21–29, 2002.

11. **Kent BB, Drane JW, Blumenstein B, and Manning JW.** A mathematical model to assess changes in the baroreceptor reflex. *Cardiology* 57: 295–310, 1972.

12. **Ku YH and Chang YZ.** β-Endorphin- and GABA-mediated depressor effect of specific electroacupuncture surpasses pressor response of emotional circuit. *Peptides* 22: 1465–1470, 2001.

13. **Ku YH and Zou CJ.** Beta-endorphinergic neurons in nucleus arcuatus and nucleus tractus solitarii mediated depressor-bradycardia effect of

"Tinggong" 2-Hz electroacupuncture. *Acupunct Electrother Res* 18: 175–184, 1993.

14. **Legramante JM, Raimondi G, Adreani CM, Sacco S, Iellamo F, Peruzzi G, and Kaufman MP.** Group III muscle afferents evoke reflex depressor responses to repetitive muscle contractions in rabbits. *Am J Physiol Heart Circ Physiol* 278: H871–H877, 2000.

15. **Li L, Yin-Xiang C, Hong X, Peng L, and Da-Nian Z.** Nitric oxide in vPAG mediates the depressor response to acupuncture in stress-induced hypertensive rats. *Acupunct Electrother Res* 26: 165–170, 2001.

16. **Li P.** The effect of acupuncture on blood pressure: the interrelation of sympathetic activity and endogenous opeoid peptides. *Acupunct Electrother Res* 8: 45–56, 1983.

17. **Li P, Pitsillides KF, Rendig SV, Pan HL, and Longhurst JC.** Reversal of reflex-induced myocardial ischemia by median nerve stimulation: a feline model of electroacupuncture. *Circulation* 97: 1186–1194, 1998.

18. **Li P, Rowshan K, Crisostomo M, Tjen-A-Looi SC, and Longhurst JC.** Effect of electroacupuncture on pressor reflex during gastric distension. *Am J Physiol Regul Integr Comp Physiol* 283: R1335–R1345, 2002.

19. **Li P, Tjen-A-Looi S, and Longhurst JC.** Rostral ventrolateral medullary opioid receptor subtypes in the inhibitory effect of electroacupuncture on reflex autonomic response in cats. *Auton Neurosci* 89: 38–47, 2001.

20. **Lin JG, Chang SL, and Cheng JT.** Release of beta-endorphin from adrenal gland to lower plasma glucose by the electroacupuncture at Zhongwan acupoint in rats. *Neurosci Lett* 326: 17–20, 2002.

21. **Lin JG, Lo MW, Wen YR, Hsieh CL, Tsai SK, and Sun WZ.** The effect of high and low frequency electroacupuncture in pain after lower abdominal surgery. *Pain* 99: 509–514, 2002.

22. **Middlekauff HR, Yu JL, and Hui K.** Acupuncture effects on reflex responses to mental stress in humans. *Am J Physiol Regul Integr Comp Physiol* 280: R1462–R1468, 2001.

23. **Mohrman DE and Heller LJ.** *Cardiovascular Physiology* (4th ed.). New York: McGraw-Hill, 1997, p. 158–230.

24. **Moore PG, Quail AW, Cottee DB, McIlveen SA, and White SW.** Effect of fentanyl on baroreflex control of circumflex coronary conductance. *Clin Exp Pharmacol Physiol* 27: 1028–1033, 2000.

25. **Mori H, Uchida S, Ohsawa H, Noguchi E, Kimura T, and Nishijo K.** Electro-acupuncture stimulation to a hindpaw and a hind leg produces different reflex responses in sympathoadrenal medullary function in anesthetized rats. *J Auton Nerv Syst* 79: 93–98, 2000.

26. **Nishijo K, Mori H, Yosikawa K, and Yazawa K.** Decreased heart rate by acupuncture stimulation in humans via facilitation of cardiac vagal activity and suppression of cardiac sympathetic nerve. *Neurosci Lett* 227: 165–168, 1997.

27. **Ohsawa H, Okada K, Nishijo K, and Sato Y.** Neural mechanism of depressor responses of arterial pressure elicited by acupuncture-like stimulation to a hindlimb in anesthetized rats. *J Auton Nerv Syst* 51: 27–35, 1995.

28. **Ohsawa H, Yamaguchi S, Ishimaru H, Shimura M, and Sato Y.** Neural mechanism of pupillary dilation elicited by electro-acupuncture stimulation in anesthetized rats. *J Auton Nerv Syst* 64: 101–106, 1997.

29. **Petty MA and Reid JL.** The effect of opiates on arterial baroreceptor reflex function in the rabbit. *Naunyn Schmiedebergs Arch Pharmacol* 319: 206–211, 1982.

30. **Richter A, Herlitz J, and Hjalmarson A.** Effect of acupuncture in patients with angina pectoris. *Eur Heart J* 12: 175–178, 1991.

31. **Sato T, Kawada T, Inagaki M, Shishido T, Takaki H, Sugimachi M, and Sunagawa K.** New analytic framework for understanding sympathetic baroreflex control of arterial pressure. *Am J Physiol Heart Circ Physiol* 276: H2251–H2261, 1999.

32. **Si QM, Wu GC, and Cao XD.** Effects of electroacupuncture on acute cerebral infarction. *Acupunct Electrother Res* 23: 117–124, 1998.

33. **Sved AF, Ito S, and Madden CJ.** Baroreflex dependent and independent roles of the caudal ventrolateral medulla in cardiovascular regulation. *Brain Res Bull* 51: 129–133, 2000.

34. **Tam KC and Yiu HH.** The effect of acupuncture on essential hypertension. *Am J Chin Med* 3: 369–375, 1975.

35. **Taneyama C, Goto H, Kohno N, Benson KT, Sasao J, and Arakawa K.** Effects of fentanyl, diazepam, and the combination of both on arterial baroreflex and sympathetic nerve activity in intact and baro-denervated dogs. *Anesth Analg* 77: 44–48, 1993.

36. **Tjen-A-Looi SC, Li P, and Longhurst JC.** Prolonged inhibition of rostral ventral lateral medullary premotor sympathetic neurons by electroacupuncture in cats. *Auton Neurosci* 106: 119–131, 2003.

37. Tjen-A-Looi SC, Peng L, and Longhurst JC. Medullary substrate and differential cardiovascular responses during stimulation of specific acupoints. *Am J Physiol Regul Integr Comp Physiol* 287: R852–R862, 2004.

38. Wang JD, Kuo TB, and Yang CC. An alternative method to enhance vagal activities and suppress sympathetic activities in humans. *Auton Neurosci* 100: 90–95, 2002.

39. Wong AM, Leong CP, Su TY, Yu SW, Tsai WC, and Chen CP. Clinical trial of acupuncture for patients with spinal cord injuries. *Am J Phys Med Rehabil* 82: 21–27, 2003.

40. Wong AM, Su TY, Tang FT, Cheng PT, and Liaw MY. Clinical trial of electrical acupuncture on hemiplegic stroke patients. *Am J Phys Med Rehabil* 78: 117–122, 1999.

41. Yamamoto K, Kawada T, Kamiya A, Takaki H, Miyamoto T, Sugimachi M, and Sunagawa K. Muscle mechanoreflex induces the pressor response by resetting the arterial baroreflex neural arc. *Am J Physiol Heart Circ Physiol* 286: H1382–H1388, 2004.

42. Yao T. Acupuncture and somatic nerve stimulation: mechanism underlying effects on cardiovascular and renal activities. *Scand J Rehabil Med Suppl* 29: 7–18, 1993.
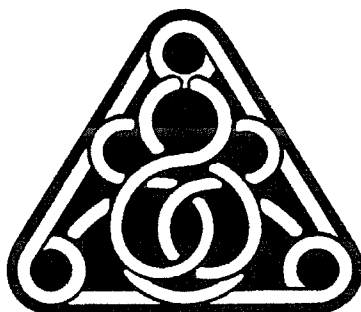
TRANSLATIONAL PHYSIOLOGY

Automated drug delivery system to control systemic arterial pressure, cardiac output, and left heart filling pressure in acute decompensated heart failure

Kazunori Uemura,[1] Atsunori Kamiya,[1] Ichiro Hidaka,[1] Toru Kawada,[1] Shuji Shimizu,[1] Toshiaki Shishido,[1] Makoto Yoshizawa,[2] Masaru Sugimachi,[1] and Kenji Sunagawa[3]

[1]*Department of Cardiovascular Dynamics, National Cardiovascular Center Research Institute, Suita;* [2]*Research Division on Advanced Information Technology, Information Synergy Center, Tohoku University, Sendai;* [3]*Department of Cardiovascular Medicine, Kyushu University Graduate School of Medical Science, Fukuoka, Japan*

Uemura, Kazunori, Atsunori Kamiya, Ichiro Hidaka, Toru Kawada, Shuji Shimizu, Toshiaki Shishido, Makoto Yoshizawa, Masaru Sugimachi, and Kenji Sunagawa. Automated drug delivery system to control systemic arterial pressure, cardiac output, and left heart filling pressure in acute decompensated heart failure. *J Appl Physiol* 100: 1278–1286, 2006. First published December 22, 2005; doi:10.1152/japplphysiol.01206.2005.—Pharmacological support with inotropes and vasodilators to control decompensated hemodynamics requires strict monitoring of patient condition and frequent adjustments of drug infusion rates, which is difficult and time-consuming, especially in hemodynamically unstable patients. To overcome this difficulty, we have developed a novel automated drug delivery system for simultaneous control of systemic arterial pressure (AP), cardiac output (CO), and left atrial pressure (Pla). Previous systems attempted to directly control AP and CO by estimating their responses to drug infusions. This approach is inapplicable because of the difficulties to estimate simultaneous AP, CO, and Pla responses to the infusion of multiple drugs. The circulatory equilibrium framework developed previously (Uemura K, Sugimachi M, Kawada T, Kamiya A, Jin Y, Kashihara K, and Sunagawa K. *Am J Physiol Heart Circ Physiol* 286: H2376–H2385, 2004) indicates that AP, CO, and Pla are determined by an equilibrium of the pumping ability of the left heart (S_L), stressed blood volume (V), and systemic arterial resistance (R). Our system directly controls S_L with dobutamine, V with dextran/furosemide, and R with nitroprusside, thereby controlling the three variables. We evaluated the efficacy of our system in 12 anesthetized dogs with acute decompensated heart failure. Once activated, the system restored S_L, V, and R within 30 min, resulting in the restoration of normal AP, CO, and Pla. Steady-state deviations from target values were small for AP [4.4 mmHg (SD 2.6)], CO [5.4 ml·min^{-1}·kg^{-1} (SD 2.4)] and Pla [0.8 mmHg (SD 0.6)]. In conclusion, by directly controlling the mechanical determinants of circulation, our system has enabled simultaneous control of AP, CO, and Pla with good accuracy and stability.

computers; negative feedback; circulatory equilibrium

IN THE MANAGEMENT OF PATIENTS with acute decompensated heart failure after myocardial infarction or after cardiac surgical procedures, cardiovascular agents such as inotropes and/or vasodilators are commonly used to control systemic arterial pressure (AP), cardiac output (CO), and left heart filling pressure (2, 13, 20). Because responses to these agents vary between patients and within patient over time, strict monitoring of patient condition and frequent adjustments of drug infusion rates are usually required. This is a difficult and time-consuming process, especially in hemodynamically unstable patients. Several closed-loop systems to automate drug infusion have been developed to facilitate this process (10, 11, 18, 26, 27). Closed-loop control of AP with vasodilators was more precise and stable than manual controls (10, 11). Chitwood et al. (10) demonstrated that, compared with manual control, closed-loop control of postoperative hypertension significantly improves patient outcome by reducing the transfusion requirement and postoperative blood loss. Although closed-loop control of hemodynamics has been suggested to be useful in clinical settings, no closed-loop system so far developed is capable of controlling the overall hemodynamics; i.e., controlling AP, CO, and left heart filling pressure simultaneously (18). This is because all previous systems attempted to directly control the hemodynamic variable by estimating response of the variable to drug infusion (10, 11, 18, 26, 27). Although such an approach worked well in controlling a single variable, it cannot be applied to control of the three variables, because it is difficult to simultaneously estimate their responses to the infusions of multiple drugs.

In this study, we developed a new automated drug delivery system that is capable of controlling AP, CO, and left atrial pressure (Pla). We modeled the entire cardiovascular system by extending Guyton's framework of circulatory equilibrium (16, 17, 24, 25). As shown in Fig. 1, the extended framework consists of an integrated cardiac output curve characterizing the pumping ability of the left and the right heart and a venous return surface characterizing the venous return property of the systemic and pulmonary circulation (24, 25). The intersection point of the integrated CO curve and the venous return surface predicts the equilibrium point of CO, Pla, and right atrial pressure (Pra) (Fig. 1) (24, 25). Once CO, Pla, and Pra are predicted from the intersection point, systemic arterial resistance determines AP. On the basis of this framework, instead of directly controlling AP, CO, and Pla, our system controls the integrated CO curve with dobutamine (Dob), the venous return surface with 10% dextran 40 (Dex) and furosemide (Fur), and systemic arterial resistance with sodium nitroprusside (SNP), thereby controlling the three hemodynamic variables.
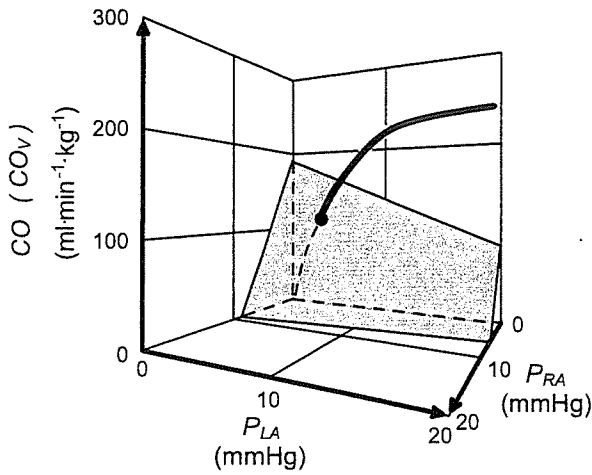
Fig. 1. Diagram of circulatory equilibrium for cardiac output (CO), venous return (COv), left atrial pressure (Pla), and right atrial pressure (Pra). The equilibrium CO, Pla, and Pra are obtained as the intersection point of the venous return surface and integrated cardiac output curve. [Modified from Uemura et al. (Ref 25).]

The purpose of this study was, therefore, to develop and validate the new automated drug delivery system. We evaluated the efficacy of our system in a canine model of acute ischemic heart failure. Our results indicated that this novel automated drug

delivery system was able to control AP, CO, and Pla simultaneously with reasonably good accuracy and stability.

METHODS

Cardiac Output Curve, Venous Return Surface, and Arterial Resistance

On the basis of previous studies, we parameterized the integrated CO curve by the pumping ability of the left heart (S_L), the venous return surface by total stressed blood volume (V), and the systemic arterial resistance by R (see APPENDIX A) (24, 25). Our system aims to control these cardiovascular parameters to achieve target AP (AP*), target CO (CO*), and target Pla (Pla*).

Automated Drug Delivery System

Figure 2A illustrates a block diagram of the automated drug delivery system, using a negative feedback mechanism.

Target values of S_L (S_L*), V (V*), and R (R*) are determined according to the AP*, CO*, and Pla* (see APPENDIX B). The subject's S_L, V, and R are calculated from the measured AP, CO, Pla, and Pra (Fig. 2A). S_L, V, and R are compared with S_L*, V*, and R*, respectively.

To minimize the difference between S_L* and S_L ($\Delta S_L = S_L$* $- S_L$) and the difference between R* and R ($\Delta R = R$* $- R$), proportional-integral (PI) feedback controllers adjusts infusion rates of Dob and SNP, respectively (Fig. 2A). In the PI controller (Fig. 2B), ΔS_L (or ΔR) and the difference integrated with an integral gain (K_i) are summed and scaled by a proportional gain (K_p) to give the infusion rate of Dob (or SNP). We determined values of K_i and K_p on the

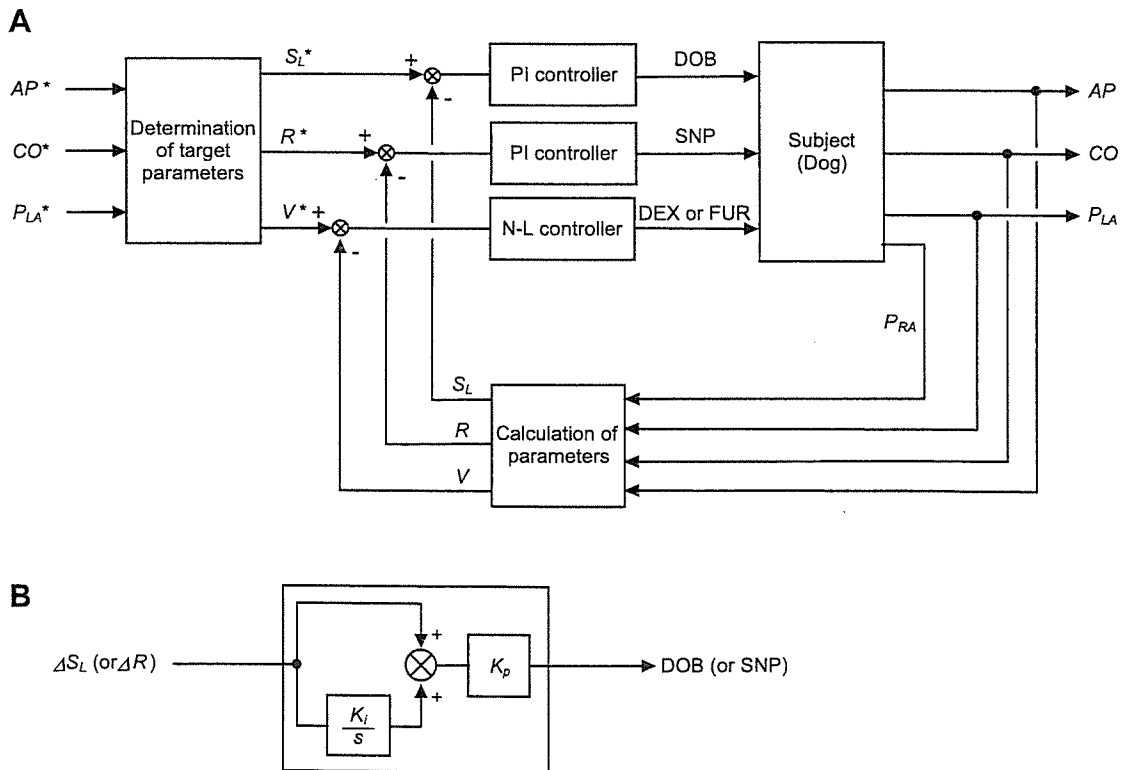
Fig. 2. A: block diagram of an automated drug delivery system for simultaneous control of systemic arterial pressure (AP), CO, and Pla. AP*, CO* and Pla* represent target AP, target CO, and target Pla, respectively. From these target variables, target values of pumping ability of the left heart (S_L*), stressed blood volume (V*), and systemic arterial resistance (R*) are determined. Subject's S_L, V, and R are calculated from measured AP, CO, Pla, and Pra. Proportional-integral (PI) controllers adjust infusion rate of dobutamine (Dob) and sodium nitroprusside (SNP) to minimize the difference between S_L and S_L* (ΔS_L), and the difference between R and R* (ΔR), respectively. Nonlinear (N-L) controller adjusts infusion of 10% dextran 40 (Dex) or injection of furosemide (Fur) so that the difference between V and V* is minimized. B: block diagram of the PI controller. K_i and K_p represent the integral and proportional gain constants, respectively; s is a Laplace operator.

basis of open-loop response of S_L (or R) to the infusion of Dob (or SNP) (4, 9).

To minimize the difference between V^* and V ($\Delta V = V^*$-V), a nonlinear (NL) feedback controller (Fig. 2A) adjusts the infusion of Dex or injection of Fur on the basis of the following "if-then" rules:

Rule 1: If $\Delta V \geq X_1$ ml/kg then infuse Dex (Y_1, ml/min)

Rule 2: If $\Delta V \leq X_2$ ml/kg then inject Fur (Y_2, mg)

We determined values of X_1, Y_1, X_2, and Y_2 on the basis of the open-loop response of V to the infusion of Dex and Fur.

These adjustment processes are repeated in parallel and continued until the differences disappear.

Preparation

We used 35 adult mongrel dogs in this study [both sexes, body weight 25 kg (SD 4)]. Care of the animals was in strict accordance with the guiding principles of the Physiological Society of Japan. All protocols were approved by the Animal Subjects Committee of the National Cardiovascular Center. Anesthesia was induced with pentobarbital sodium (25 mg/kg). Animals were intubated endotracheally. Isoflurane (1.0%) was inhaled continuously to maintain an appropriate level of anesthesia during the experiment. A catheter (8-Fr) was placed in the right femoral artery, which was connected to a pressure transducer (DX-200, Nihon Kohden, Tokyo, Japan) to measure AP. After a median sternotomy, a small pericardial incision was made at the level of the aortic root. Through the incision, an ultrasonic flow meter (20A594, Transonics, Ithaca, NY) was placed around the ascending aorta to measure CO. Fluid-filled catheters were placed in the left and right atria to measure Pla and Pra, respectively. They were connected to pressure transducers (DX-200, Nihon Kohden). The junction between the vena cavae and the right atrium was taken as the reference point for zero pressure. The undamped natural frequency and the damping ratio of the fluid filled catheters for the pressure measurements were 21 Hz and 0.22, respectively. A urinary catheter was inserted to measure urine volume.

A catheter (6-Fr) was placed in the right femoral vein. A roller pump (Minipuls 3, Gilson, Middleton, WI) was attached to the venous line to infuse Dex. A double-lumen catheter was also introduced into the right femoral vein for administration of Dob and SNP. Infusion pumps (CFV-3200, Nihon Kohden) were used for Dob and SNP infusion. The infusion rates of Dex, Dob, and SNP were controlled with a personal computer (MA20V, NEC, Tokyo, Japan) through a 12-bit digital-to-analog converter (DA12-8PCI, Contec, Osaka, Japan). A catheter (6-Fr) was placed in the right external jugular vein, from which Fur was injected after a command signal from the computer.

Experimental Protocols

We induced left ventricular failure (LVF) in all the animals by embolizing the left circumflex coronary artery with glass microspheres (90 μm in diameter) (24, 25). We adjusted the amount of injected microspheres to increase Pla to more than 18 mmHg or decrease CO to less than 70 ml·min⁻¹·kg⁻¹. When ventricular tachycardia or frequent premature ventricular contractions were noted, lidocaine (1 mg/min) was infused to suppress the arrhythmia.

Response of cardiovascular parameters to drug infusion. Under open-loop conditions, we examined the response of cardiovascular parameters to drug infusions in 21 dogs with LVF. In 10 dogs, we infused Dob in a stepwise manner at 6 μg·kg⁻¹·min⁻¹ for 10 min to obtain a step response of S_L. In six dogs, we infused SNP at 2 μg·kg⁻¹·min⁻¹ for 10 min to obtain a step response of R. In five dogs, we infused Dex at 0.4 ml·min⁻¹·kg⁻¹ for 10 min to observe the response of V. In seven dogs, we injected Fur (20 mg, bolus iv) and observed the response of V and urine volume for 50 min.

Application of the automated drug delivery system. We applied the system to the other 14 dogs with LVF. We first defined AP* (90–105

mmHg), CO* (90–100 ml·min⁻¹·kg⁻¹), and Pla* (8–12 mmHg), which were fed into the system to determine S_L^*, V^*, and R^* (see APPENDIX B). The controllers were then activated by closing the loops. In 12 dogs (*group 1*), we observed the performance of the system over 50–60 min. In two dogs (*group 2*), we observed the performance of the system over 100–150 min to evaluate stability of the closed-loop control over a longer periods of time.

With the use of the computer, analog signals of AP, CO, Pla, and Pra were digitized at 200 Hz with a 12-bit analog-to-digital converter [AD12-16U(PCI)E, Contec, Osaka, Japan] and stored on a hard disk for offline analysis. In the closed-loop control, the digitized signals were smoothed by a low-pass filter (time constant, 10 s) and were used as the system controlled variables. The infusion rates of Dob, SNP, and Dex were also stored. Urine volume after the injection of Fur was recorded.

Data Analysis

Evaluation of the response of cardiovascular parameters and design of the controller. We described the step response of S_L and R by a transfer function of a first-order model with a transport delay. In this model, change in S_L from baseline (δS_L) in response to Dob infusion can be expressed by the following formula:

$$\delta S_L(t) = \begin{cases} G \cdot \left[1 - \exp\left(-\frac{t-L}{T} \right) \right] & (t \geq L) \\ 0 & (t < L) \end{cases} \quad (1)$$

where G is static gain [ml·min⁻¹·kg⁻¹(μg·kg⁻¹·min⁻¹)⁻¹], L is transport delay (s), and T is time constant (s). Change in R from baseline (δR) in response to the SNP infusion can be expressed similarly and is characterized by G [mmHg·min·ml⁻¹·kg (μg·kg⁻¹·min⁻¹)⁻¹], L (s), and T (s). We estimated the parameters of the transfer function by approximating δS_L and δR to *Eq. 1* using the least square method. We averaged the parameters of the transfer function of S_L response for 10 animals and those of R response for 6 animals. The averaged parameters were used to determine the PI gain constants, K_i and K_p, in accordance with the method of Chien et al. (9). Their method provides PI constants that permit the regulated variable to respond rapidly without overshoot (4, 9).

We evaluated the change in V from baseline (δV) in response to the infusion of Dex and Fur. On the basis of δV, we determined the constants (X_1, Y_1, X_2, and Y_2) of the if-then rules.

Efficacy of the automated drug delivery system. We calculated the following indexes to evaluate the accuracy and stability of the control of AP, CO, and Pla by the new system: the time required for the hemodynamic variables to reach the acceptable ranges of the target values (± 10 mmHg for AP, ± 10 ml·min⁻¹·kg⁻¹ for CO, ± 2 mmHg for Pla), and the standard deviations of the steady-state differences between AP and AP*, between CO and CO*, and between Pla and Pla*. Because steady states were reached within 30 min in all the variables in the present study, standard deviations were calculated from 30 min after the loop was closed.

Statistics

Group data are expressed as means (SD) unless otherwise stated. Student's paired *t*-test was used to compare hemodynamic data at baseline and after the coronary embolization. One-way ANOVA with Tukey's post hoc test was used to compare hemodynamic data before, during, and after the closed-loop control of hemodynamics. The level of statistical significance was defined as $P < 0.05$.

RESULTS

Hemodynamic data at baseline and after left circumflex coronary artery embolization are summarized in Table 1. Coronary embolization more than doubled Pla [from 7.5 (SD 1.9) to 19.4 (SD 6.2) mmHg] and halved CO [from 131.4 (SD

Table 1. *Hemodynamic data at baseline and after left circumflex coronary artery embolization*

	Baseline	Embolization
HR, beats/min	141.3 (19.5) [112.0–188.3]	146.2 (28.8) [81.4–197.9]
AP, mmHg	109.1 (18.7) [76.4–140.0]	90.9 (16.5) [66.9–135.6]*
CO, ml·min^{-1}·kg^{-1}	131.4 (40.9) [64.5–229.2]	66.8 (23.3) [30.3–121.7]*
Pla, mmHg	7.5 (1.9) [4.7–12.8]	19.4 (6.2) [7.9–34.5]*
Pra, mmHg	4.2 (1.2) [2.1–7.2]	6.0 (1.8) [3.5–9.9]*
S_L, ml·min^{-1}·kg^{-1}	54.3 (18.1) [25.2–105.9]	19.1 (7.6) [8.0–33.7]*
R, mmHg·min·ml^{-1}·kg	0.9 (0.4) [0.4–1.8]	1.4 (0.5) [0.7–2.6]*
V, ml/kg	31.0 (6.6) [21.7–45.2]	32.3 (4.9) [20.6–43.7]

Values are means (SD) ($n = 35$ in each group). Numbers in brackets are the ranges. HR, heart rate. AP, systemic arterial pressure; CO, cardiac output; Pla, left atrial pressure; Pra, right atrial pressure; S_L, pumping ability of the left heart; R, systemic arterial resistance; V, stressed blood volume. *$P < 0.01$ vs. baseline.

40.9) to 66.8 (SD 23.3) ml·min^{-1}·kg^{-1}]. This decreased S_L to about one-third of the baseline value, which indicates substantial downward shift of the left cardiac output curve. These changes are compatible with severe LVF.

Response of Cardiovascular Parameters to Drug Infusion

Figure 3 shows the open-loop responses of cardiovascular parameters to drug infusions. Figure 3, *A* and *B*, shows the averaged time course of δS_L during Dob infusion ($n = 10$)

and that of δR during SNP infusion ($n = 6$), respectively. Dob infusion increased δS_L, and SNP infusion decreased δR exponentially. The results of the fit of δS_L and δR to *Eq. 1* are summarized in Table 2. The fact that the correlation coefficients were close to unity, with a small standard error of the estimate relative to the amount of δS_L and δR, suggested that the approximation of δS_L and δR to *Eq. 1* was reasonably accurate. On the basis of the averaged parameters of the transfer function (Table 2), we determined the PI gain constants for Dob infusion [$K_i = 0.01$ s^{-1}, $K_p = 0.06$ μg·kg^{-1}·min^{-1} (ml·min^{-1}·kg^{-1})$^{-1}$] and for SNP infusion [$K_i = 0.007$ s^{-1}, $K_p = -1.37$ μg·kg^{-1}·min^{-1} (mmHg·min·ml^{-1}·kg)$^{-1}$].

Figure 3*C* shows the averaged time course of δV in response to Dex infusion ($n = 5$). δV increased and plateaued [7.2 ml/kg (SD 2.2)] after the cessation of Dex infusion. δV at the plateau was greater than the total volume of Dex infused (4 ml/kg), suggesting transvascular fluid absorption by colloid osmotic pressure (3). Figure 3*D* shows the averaged time course of δV after a single intravenous injection of Fur (20 mg, $n = 7$). δV gradually decreased and reached a trough [-4.3 ml/kg (SD 3.5)] around 30 min after the Fur injection. Average urine volume was 180 ml (SD 94). On the basis of these responses, we determined the constants of the if-then rules as $X_1 = 1$ ml/kg, $Y_1 = 10$ ml/min, $X_2 = -2$ ml/kg, and $Y_2 = 10$ mg. To avoid oscillation between hypovole-
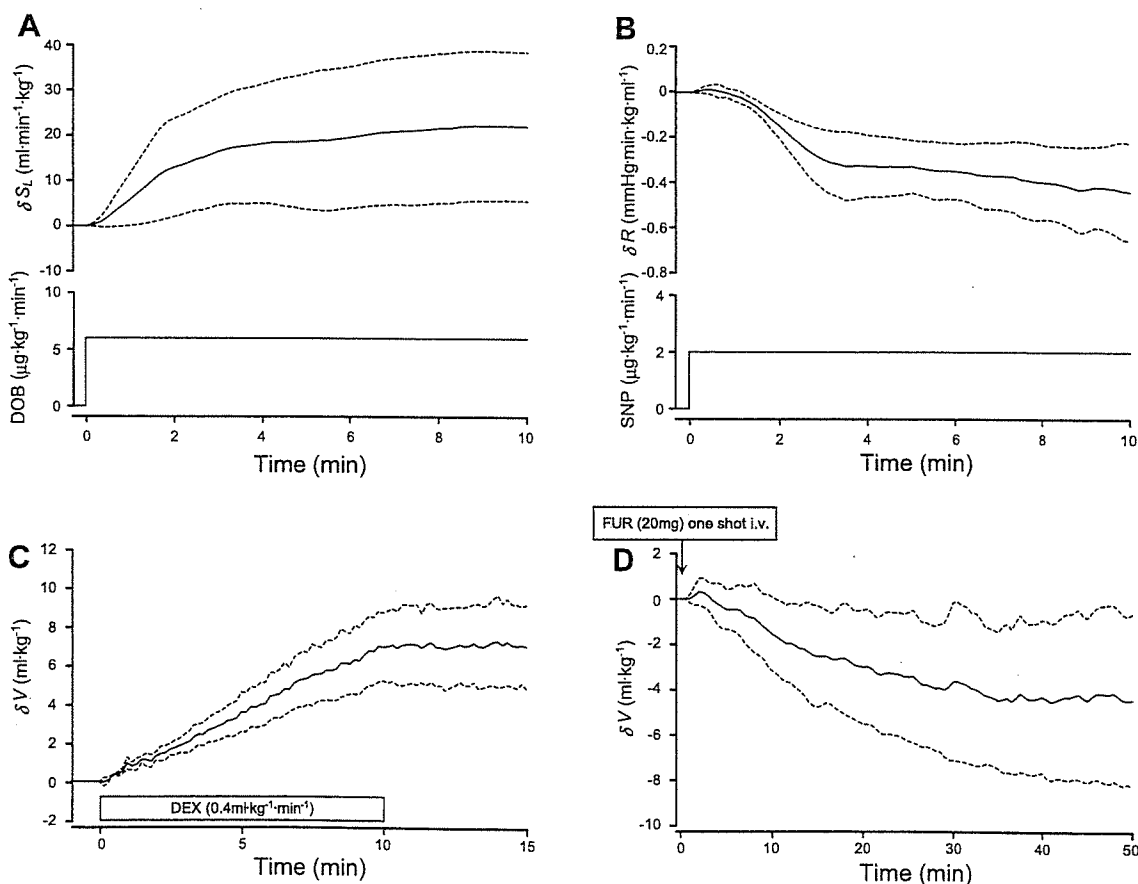

Fig. 3. Response of cardiovascular parameter to drug infusion. *A*: averaged response of S_L to stepwise Dob infusion (6 μg·kg^{-1}·min^{-1}) ($n = 10$). The ordinate indicates change in S_L from baseline (δS_L). *B*: averaged response of R to stepwise SNP infusion (2 μg·kg^{-1}·min^{-1}) ($n = 6$). The ordinate indicates change in R from baseline (δR). *C* and *D*: averaged response of V to Dex infusion (0.4 ml·min^{-1}·kg^{-1}) (*C*, $n = 5$) and to Fur (20 mg) injection (*D*, $n = 7$). The ordinates indicate change in V from baseline (δV). Data are expressed by mean (solid line) ± SD (broken line).

Table 2. *Parameters of step response of S_L and R*

	G	L	T	r	SEE
δS_L	3.6 (2.7)	63.5 (46.9)	79.0 (78.0)	0.91 (0.09)	2.0 (0.7)
δR	−0.21 (0.08)	69.8 (26.1)	117.1 (80.2)	0.93 (0.02)	0.06 (0.02)

Values are means (SD). δS_L, change in S_L from baseline; δR, change in R from baseline; G, static gain of δS_L [ml·min^{-1}·kg^{-1} (μg·kg^{-1}·min^{-1})$^{-1}$] and of δR [mmHg·min·ml^{-1}·kg (μg· kg^{-1}·min^{-1})$^{-1}$]; L, transport delay (s); T, time constant (s); r, correlation coefficient; SEE, standard error of the estimate of δS_L (ml·min^{-1}·kg^{-1}) and of δR (mmHg·min·ml^{-1}·kg).

mia and hypervolemia (hence infusion of Dex and injection of Fur), we introduced a dead zone (−2 ml/kg < ΔV < 1 ml/kg) into the rules (4). We set continuous checking for *rule 1* and checking at 20-min intervals for *rule 2*.

With the controllers thus designed, we evaluated the performance of the automated system in the next protocol.

Performance of the Automated Drug Delivery System

Figure 4 shows the experimental trial in a representative case. The automated system was activated at 0 min. Figure 4A shows the time courses of the infusion rates of Dob and SNP and the accumulated volume of infused Dex. In this case, Fur was not injected. Figure 4B shows the time courses of S_L, R, and V. Infusion rates of Dob, SNP, and Dex were adjusted so that S_L, R, and V reached their respective target values. By controlling the cardiovascular parameters, the automated system controlled AP, CO, and Pla accurately and stably as demonstrated in Fig. 4C. AP, CO, and Pla reached their respective target levels within 30 min and remained at these levels.

Figure 5 summarizes the results obtained for 12 dogs (*group 1*), demonstrating the effectiveness of the performance of the automated system. Figure 5A shows averaged time courses of

the infusion rates of Dob and SNP, and the accumulated volume of infused Dex. The average infusion rates of Dob and SNP were 4.7 μg·kg^{-1}·min^{-1} (SD 2.6) and 4.2 μg·kg^{-1}·min^{-1} (SD 1.8), respectively. The average volume of infused Dex was 2.4 ml/kg (SD 1.9). Fur was injected once in one animal and twice in another animal. In these two animals, V decreased by 3.8–10.2 ml/kg in response to the injection of Fur with a total urine volume of 250–300 ml. Figure 5B shows averaged time courses of difference between S_L and S_L* (S_L − S_L*), difference between R and R* (R − R*), and difference between V and V* (V − V*). Once the system was activated, these differences rapidly converged to the zero lines in all the animals. S_L was restored to subnormal conditions [33.0 ml·min^{-1}·kg^{-1} (SD 2.6)] irrespective of the magnitude of depression before the control [13.8 ml·min^{-1}·kg^{-1} (SD 3.5), from 9.4 to 20.5 ml·min^{-1}·kg^{-1}]. These resulted in accurate and stable control of AP, CO, and Pla (Fig. 5C). The ordinates of Fig. 5C indicate the difference between AP and AP* (AP − AP*), difference between CO and CO* (CO − CO*), and difference between Pla and Pla* (Pla − Pla*). These differences also converged to the zero lines rapidly. The average times for AP, CO, and Pla to reach the acceptable ranges were 5.2 min (SD 6.6), 6.8 min (SD 4.6), and 11.7 min (SD 9.8),
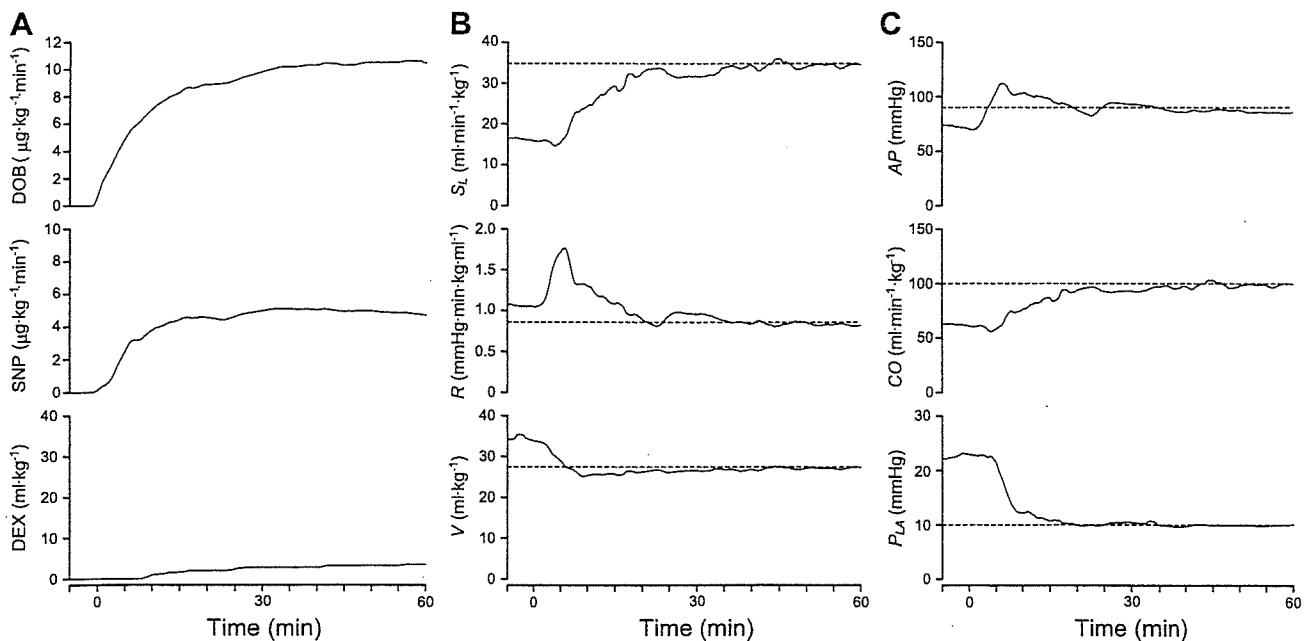

Fig. 4. Time courses of infusion rates of Dob and SNP, and cumulated volume of infused Dex (A), cardiovascular parameters (B), and hemodynamic variables (C) in 1 representative animal during closed-loop control of hemodynamics. Broken horizontal lines in B indicate target parameters (*top*, S_L*; *middle*, R*; *bottom*, V*). Broken horizontal lines in C indicate target hemodynamic variables (*top*, AP*; *middle*, CO*; *bottom*, Pla*). Drug infusion rates were adjusted so that the cardiovascular parameters reached the respective target values. As the parameters got closer to their targets, all 3 hemodynamic variables approached their respective target values.
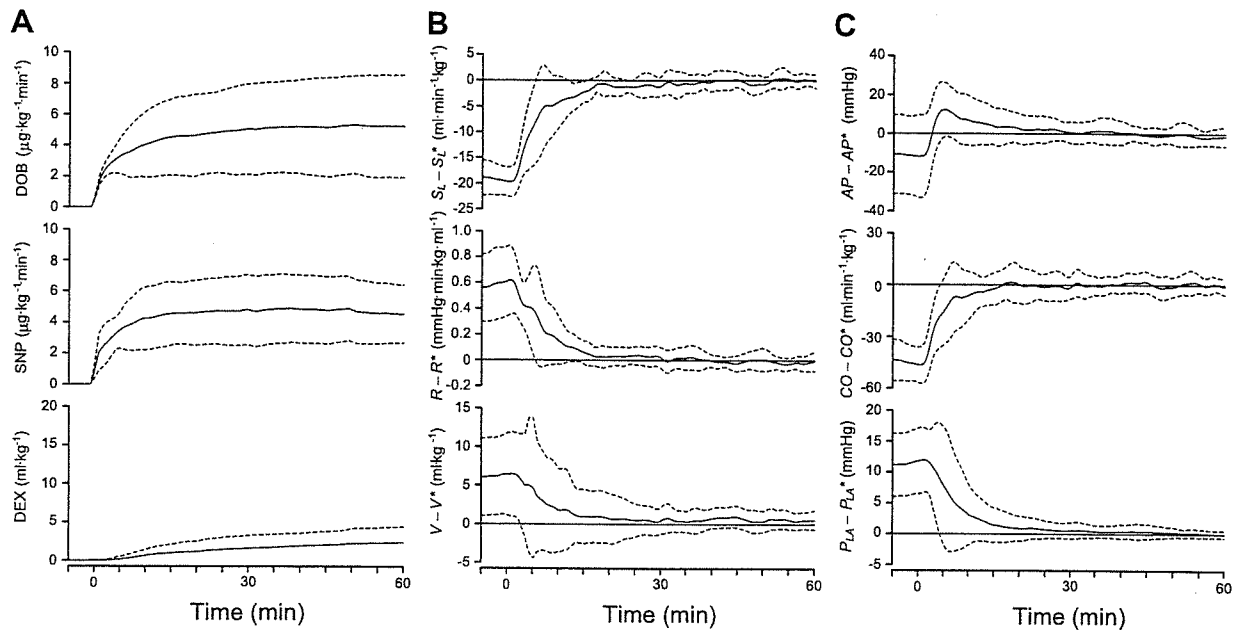
Fig. 5. Time courses of infusion rates of Dob and SNP, and cumulated volume of infused Dex (A), differences between measured and target cardiovascular parameters (B), and differences between measured and target hemodynamic variables (C) averaged for 12 dogs during closed-loop control of hemodynamics. Data are expressed as mean (solid line) ± SD (broken line). As the differences between measured and target parameters converged to the zero lines, the differences between measured and target hemodynamic variables also converged to the zero lines and remained at those levels.

respectively. The average standard deviations from the target values were small for AP [4.4 mmHg (SD 2.6)], CO [5.4 ml·min^{-1}·kg^{-1} (SD 2.4)] and Pla [0.8 mmHg (SD 0.6)]. In case of severe hypotension, restoring normal AP should be done within a few minutes to prevent cerebral ischemia. Four of 12 dogs exhibited severe hypotension [AP, 67 mmHg (SD 6)]. In these animals, AP* [95 mmHg (SD 4)] was attained within 4 min [mean 2.8 min (SD 0.7)]. Hemodynamic data before, during, and after the closed-loop control of hemodynamics are summarized in Table 3. After the system was turned off, AP, CO, and Pla gradually returned to their precontrol levels in 11 animals. In one animal, however, progressive hypotension followed by intractable ventricular fibrillation occurred ~3 min after the system was turned off.

In two dogs (group 2), AP, CO, and Pla were controlled with reasonable stability over a longer periods of time (100–150 min). Standard deviations from target values were small for AP (3.9–7.8 mmHg), CO (2.7–6.6 ml·min^{-1}·kg^{-1}), and Pla (0.7–2.5 mmHg).

Table 3. *Hemodynamic data before, during, and after the closed-loop control of hemodynamics*

	Before (n = 12)	During (n = 12)	After (n = 11)
HR, beats/mm	147.4 (26.8)	149.4 (25.0)	135.7 (25.2)†‡
AP, mmHg	86.7 (22.4)	97.0 (7.4)	75.2 (21.1)‡
CO, ml·min^{-1}·kg^{-1}	53.7 (14.6)	96.7 (5.3)†	53.5 (8.6)‡
Pla, mmHg	21.8 (5.5)	10.8 (1.2)†	18.5 (3.4)‡
Pra, mmHg	6.9 (1.8)	4.4 (0.9)†	7.4 (2.2)‡
S$_L$, ml·min^{-1}·kg^{-1}	14.3 (4.0)	32.7 (2.6)†	15.1 (2.9)‡
R, mmHg·min·ml^{-1}·kg	1.5 (0.3)	1.0 (0.1)†	1.3 (0.4)*‡
V, ml/kg	34.2 (4.9)	28.5 (2.3)†	34.0 (5.4)‡

Values are means (SD). *$P < 0.05$, †$P < 0.01$ vs. Before; ‡$P < 0.01$ vs. During.

DISCUSSION

To the best of our knowledge, the automated drug delivery system we have developed is the first to successfully control AP, CO, and Pla simultaneously with reasonably good accuracy and stability. In a canine model of acute heart failure, our system automatically normalizes AP, CO, and Pla and maintains the levels stably within the desired ranges. Therefore, our system is potentially useful in the management of patients with acute decompensated heart failure.

Previous Closed-Loop Systems Controlling Hemodynamic Variables

Several previous systems have attempted to control two hemodynamic variables simultaneously (18, 26, 27). However, it is difficult to expand them to closed-loop control of the overall hemodynamics.

Voss et al. (26) and Yu et al. (27) reported closed-loop systems to control AP and CO using inotropes and vasodilators in dogs. In these systems, all possible input-output relations between drug infusion and the response of the controlled variable have to be estimated; namely, inotrope-AP, inotrope-CO, vasodilator-AP, and vasodilator-CO relations. The reason for this is that these drugs affect AP and CO simultaneously to almost the same degree. If this approach is applied to simultaneous control of AP, CO, and Pla, at least nine input-output relations have to be estimated, because at least three drugs are required to independently control the three variables. This would make the system extremely complicated and therefore be practically unfeasible.

In addition, the input-output relations must be estimated online in individual animals to tune the drug controllers. The reason for this is that the relations differ widely between animals and within animal over time. Even the direction of the

output response can change. For example, CO usually increases in response to SNP infusion in subjects with failing hearts but may also decrease in subjects with preserved cardiac function (23, 26). In the closed-loop system of Voss et al., such estimation induced unacceptably large fluctuations in AP (26). The feasibility of such online estimation is questionable when drug infusion rates are allowed to vary simultaneously because of the difficulty to differentiate between drug effects. To avoid this problem, Hoeksel et al. (18) allowed only one drug to be varied at a time, whereas other drugs were kept constant in closed-loop control of AP and pulmonary arterial pressure during cardiac surgery. However, their adjustments of volume supplementation or dobutamine infusion were manual. Their system did not completely automate the control of hemodynamics.

Characteristics of Our System

Our system controls the cardiovascular parameters characterizing the integrated CO curve, venous return surface, and arterial resistance and as a result achieves target values for hemodynamic variables. Compared with previous systems, our system may appear to adopt a rather roundabout approach. Our concept is that controlling the cardiovascular parameters is physiologically more rational, because it is equivalent to directly controlling the mechanical determinants of circulation. As indicated by Guyton et al. (16, 17), when the mechanics of the circulation are considered, the hemodynamic variables such as AP, CO, and atrial pressures are the effects, or dependent variables. Blood volume and the mechanical properties of the heart and vasculature, such as heart rate, ventricular contractility, and vascular resistance, are the causes, or independent variables. The integrated CO curve and venous return surface display these properties through the relationship between the flow and atrial pressures (24, 25). The total artificial heart control system developed by Abe et al. (1) adjusted its output in accordance with the vascular conductance (1/resistance) and AP, thereby achieving appropriate response to peripheral metabolic demands and avoiding hemodynamic abnormalities exhibited by other total artificial heart control systems. Their results also suggest that it is essential to consider the mechanical determinant of circulation for the control of the hemodynamic variables.

Our approach is advantageous from the perspective of control engineering. The three drug controllers (Fig. 2A) are designed on the basis of only four input-output relations between the drug infusion and the response of the controlled parameter; namely, Dob-S_L, SNP-R, Dex-V, and Fur-V (Fig. 3). We also found that Dob decreases R and increases V, and SNP increases S_L and decreases V (data not shown), which are compatible with previous studies (7, 22, 23). If these secondary effects induce significant interactions among the three closed loops, additional controllers would be needed to compensate for the interactions (4). However, our results indicate that these secondary effects are small enough to be compensated by the three drug controllers, and additional controllers are not necessary. The fact that the three closed loops are effectively decoupled drastically simplifies the entire system. This also permits system operators to understand its behavior easily (4).

Although we fix the PI gain constants and the constants of if-then rules, controls of cardiovascular parameters are accu-

rate and stable (Fig. 4B). There are interindividual differences in the response of the parameters to drug infusion (Fig. 3). There should also be intraindividual differences in the response over time. However, our results indicate that the three drug controllers effectively compensate for all of these differences and do not require adaptive tuning in individual animals as in the previous system. As long as each cardiovascular parameter responds sensitively to the corresponding agent, our system is able to achieve target values for all the parameters, thereby achieving target hemodynamic variables.

Our system explicitly quantifies cardiac pump function, preload, and afterload, thereby controlling the overall hemodynamics. We believe that this unique feature of our system is intuitively appealing and is acceptable to clinicians.

Clinical Application of Our System

Our system will reduce the stress and work imposed on physicians and nurses who are managing patients with unstable hemodynamic conditions. These personnel will be able to spend more time on other patient-related activities, thereby improving the quality of patient care (10, 11). We believe that the closed-loop control of overall hemodynamics can extend the improvement in postoperative outcome demonstrated by Chitwood et al. (10) to various aspects of clinical cardiology or cardiac surgery.

In clinical settings, multisystem disorders such as renal disease, anemia, and diabetes may affect the performance of our system. Renal disease can weaken the response of V to the infusion of Fur. The hemodynamic changes in anemia include increased preload and reduced arterial resistance as compensatory mechanisms for the reduced oxygen-carrying capacity of the blood (8). These changes may affect the control of V and R by our system. In patients with diabetic cardiomyopathy, the sensitivity of S_L to Dob infusion may be reduced (5). Drugs prescribed before hospitalization such as β-blockers, or used during hospitalization such as morphine may also affect the performance of our system. Chronic β-adrenergic blockade can weaken the sensitivity of S_L to Dob infusion (2). Administration of morphine may change the response of V and R to the drugs infused (15). We must clarify these effects on the performance of our system as thoroughly as possible before our system can be considered for clinical application.

In the routine clinical environment, CO, and pulmonary artery occlusion pressure, a substitute for Pla, are measured intermittently with a Swan-Ganz catheter. For clinical application of our system, it is a prerequisite to monitor these variables continuously. Several methods have been developed to continuously monitor CO or the pulmonary artery occlusion pressure (6, 12). Integrating these methods into our system would bring the clinical application of our system closer to reality.

Limitations

All the experiments of this study were conducted in anesthetized, open-chest dogs. Anesthesia and surgical trauma affect the cardiovascular system significantly. Whether the present system is efficacious in conscious, closed-chest animals (including humans) remains to be seen.

We parameterized the integrated cardiac output curve and the venous return surface using Eqs. A1, A2, and A4 (24, 25). Even if the actual curve or surface deviate slightly from those

estimated by these equations, our system compensates such deviations by the negative feedback mechanism. However, we did not confirm whether the estimation works well outside the physiological ranges of Pla and Pra, particularly under low atrial pressures (24, 25). The efficacy of our system in such conditions remains to be evaluated.

Our system controls R with vasodilators only and lacks a controller to increase R with vasoconstrictors. This will not be a major problem because the pathophysiology of acute heart failure is characterized by excessive vasoconstriction due to enhanced activity of sympathetic and renin-angiotensin systems (19). Vasoconstrictor control is necessary, however, for the management of patients with excessive vasodilatation, such as those in septic shock (21).

In this study, control of S_L was accurate and stable. However, it would be impossible to restore S_L pharmacologically if S_L is more severely depressed than those seen in this study as in the case of more diffuse myocardial disease or superimposed coronary artery disease. We must clarify in future studies to what magnitude of S_L depression can our system restore it reliably. In addition, how to use our system with mechanical circulatory support such as the intra-aortic balloon pump in case of the severe S_L depression remains to be established.

In the present design, if S_L is unable to respond to the infusion of Dob, the system will automatically increase the infusion rate of Dob owing to its negative feedback mechanism. This would be problematic especially in case of arrhythmia, which is a serious noise in the closed-loop control of S_L. If not appropriately suppressed, frequent premature ventricular contractions or ventricular tachycardia will depress S_L owing to disorganized ventricular contraction. In response to the depressed S_L, the system automatically increases the infusion rate of dobutamine. This could further exacerbate the arrhythmia, thus leading to a vicious cycle and collapse of the hemodynamics. To prevent such malfunction, a smart "sensor" that will filter these unwanted artifacts should be included in our system.

In the present study, we recorded only the urine volume. Measurement of urine flow and sodium excretion is essential to evaluate renal function, which is a very important prognostic indicator in patients with acute decompensated heart failure (14). It would be desirable to add the monitoring of these parameters to our system to improve the quality of patient care.

In conclusion, by directly controlling the mechanical determinants of circulation, our automated drug delivery system allows simultaneous control of AP, CO, and Pla with reasonable accuracy and stability and is potentially a powerful clinical tool for the management of patients with acute decompensated heart failure.

APPENDIX A

Parameters of Integrated Cardiac Output Curve, Venous Return Surface, and Arterial Resistance

We parameterized the integrated CO curve, the venous return surface and the systemic arterial resistance on the basis of previous studies (24, 25). In the integrated CO curve, CO ($ml \cdot min^{-1} \cdot kg^{-1}$) is closely related to Pla (mmHg) by the following formula (24):

$$CO = S_L \times [\ln(Pla - 2.03) + 0.80] \quad (A1)$$

and CO to Pra (mmHg) as follows:

$$CO = S_R \times [\ln(Pra - 1.0) + 0.88] \quad (A2)$$

S_L and S_R ($ml \cdot min^{-1} \cdot kg^{-1}$) are parameters representing the preload sensitivity of CO, i.e., the pumping ability of the left and right heart, respectively. These relations are consistent among different animals (24). In a preliminary study, we found that the ratio of S_R to S_L (α) remains fairly constant during infusion of dobutamine (data not shown). This suggests that once we know α, we can predict S_R in relation to a known change in S_L. Therefore we used S_L to parameterize the integrated CO curve. S_L can be calculated from CO and Pla by rewriting *Eq. A1* as follows:

$$S_L = CO/[\ln(Pla - 2.03) + 0.80] \quad (A3)$$

The venous return surface can be mathematically expressed by the following formula (25):

$$CO_V = V/0.129 - 19.61Pra - 3.49Pla \quad (A4)$$

V (ml/kg) is total stressed blood volume, and CO_V ($ml \cdot min^{-1} \cdot kg^{-1}$) is integrated venous return from systemic and pulmonary circulations. This relationship is also consistent among different animals (25). We used V to parameterize the venous return surface. V can be calculated from CO (= CO_V), Pla, and Pra by rewriting *Eq. A4* as follows:

$$V = (CO + 19.61Pra + 3.49Pla) \times 0.129 \quad (A5)$$

We parameterized the systemic arterial resistance (R) ($mmHg \cdot ml^{-1} \cdot min \cdot kg$) by the following formula:

$$R = (AP - Pra)/CO \quad (A6)$$

APPENDIX B

Determination of Target Parameters

On the basis of AP*, CO*, and Pla*, our system determines S_L*, V*, and R* as follows: S_L* is calculated by substituting CO* and Pla* into *Eq. A3*. By substituting baseline CO, Pla, and Pra into *Eqs. A1* and *A2*, baseline S_L and S_R are calculated to determine α. S_R (S_R*) corresponding to S_L* is predicted as:

$$S_R^* = \alpha \cdot S_L^* \quad (B1)$$

From *Eq. A2* and *B1*, target Pra (Pra*) is predicted as:

$$Pra^* = \exp[(CO^*)/(S_R^*) - 0.88] + 1.0 \quad (B2)$$

By substituting CO*, Pla*, and Pra* into *Eq. A5*, V* can be determined. By substituting AP*, CO*, and Pra* into *Eq. A6*, R* can be calculated.

GRANTS

REFERENCES

1. **Abe Y, Chinzei T, Mabuchi K, Snyder AJ, Isoyama T, Imanishi K, Yonezawa T, Matsuura H, Kouno A, Ono T, Atsumi K, Fujimasa I, and Imachi K.** Physiological control of a total artificial heart: conductance- and arterial pressure-based control. *J Appl Physiol* 84: 868–876, 1998.
2. **Antman EM, Anbe DT, Armstrong PW, Bates ER, Green LA, Hand M, Hochman JS, Krumholz HM, Kushner FG, Lamas GA, Mullany CJ, Ornato JP, Pearle DL, Sloan MA, and Smith SC Jr; American College of Cardiology; American Heart Association; Canadian Car-

diovascular Society. ACC/AHA guidelines for the management of patients with ST-elevation myocardial infarction—executive summary. A report of the American College of Cardiology/American Heart Association Task Force on Practice Guidelines (Writing Committee to revise the 1999 guidelines for the management of patients with acute myocardial infarction). *J Am Coll Cardiol* 44: 671–719, 2004.

3. Arakawa M, Jerome EH, Enzan K, Grady M, and Staub NC. Effects of dextran 70 on hemodynamics and lung liquid and protein exchange in awake sheep. *Circ Res* 67: 852–861, 1990.

4. Astrom KJ and Hagglund T. *PID Controller: Theory, Design, and Tuning* (2nd ed.). Research Triangle Park, NC: Instrument Society of America, 1995, p. 59–199.

5. Atkins FL, Dowell RT, and Love S. β-Adrenergic receptors, adenylate cyclase activity, and cardiac dysfunction in the diabetic rat. *J Cardiovasc Pharmacol* 7: 66–70, 1985.

6. Bein B, Worthmann F, Tonner PH, Paris A, Steinfath M, Hedderich J, and Scholz J. Comparison of esophageal Doppler, pulse contour analysis, and real-time pulmonary artery thermodilution for the continuous measurement of cardiac output. *J Cardiothorac Vasc Anesth* 18: 185–189, 2004.

7. Binkley PF, Murray KD, Watson KM, Myerowitz PD, and Leier CV. Dobutamine increases cardiac output of the total artificial heart. Implications for vascular contribution of inotropic agents to augmented ventricular function. *Circulation* 84: 1210–1215, 1991.

8. Chapler CK and Cain SM. The physiologic reserve in oxygen carrying capacity: studies in experimental hemodilution. *Can J Physiol Pharmacol* 64: 7–12, 1986.

9. Chien KL, Hrones JA, and Reswick JB. On the automatic control of generalized passive systems. *Trans ASME* 74: 175–185, 1952.

10. Chitwood WR Jr, Cosgrove DM III, and Lust RM. Multicenter trial of automated nitroprusside infusion for postoperative hypertension. Titrator Multicenter Study Group. *Ann Thorac Surg* 54: 517–522, 1992.

11. Cosgrove DM III, Petre JH, Waller JL, Roth JV, Shepherd C, and Cohn LH. Automated control of postoperative hypertension: a prospective, randomized multicenter study. *Ann Thorac Surg* 47: 678–682, 1989.

12. DeBoisblanc BP, Pellett A, Johnson R, Champagne M, McClarty E, Dhillon G, and Levitzky M. Estimation of pulmonary artery occlusion pressure by an artificial neural network. *Crit Care Med* 31: 261–266, 2003.

13. Forrester JS, Diamond G, Chatterjee K, and Swan HJ. Medical therapy of acute myocardial infarction by application of hemodynamic subsets (first of two parts). *N Engl J Med* 295: 1356–1362, 1976.

14. Gottlieb SS, Abraham W, Butler J, Forman DE, Loh E, Massie BM, O'Connor CM, Rich MW, Stevenson LW, Young J, and Krumholz HM. The prognostic importance of different definitions of worsening renal function in congestive heart failure. *J Card Fail* 8: 136–141, 2002.

15. Greenberg S, McGowan C, Xie J, and Summer WR. Selective pulmonary and venous smooth muscle relaxation by furosemide: a comparison with morphine. *J Pharmacol Exp Ther* 270: 1077–1085, 1994.

16. Guyton AC. Determination of cardiac output by equating venous return curves with cardiac response curves. *Physiol Rev* 35: 123–129, 1955.

17. Guyton AC, Coleman TG, and Granger HJ. Circulation: overall regulation. *Annu Rev Physiol* 34: 13–46, 1972.

18. Hoeksel SA, Blom JA, Jansen JR, Maessen JG, and Schreuder JJ. Automated infusion of vasoactive and inotropic drugs to control arterial and pulmonary pressures during cardiac surgery. *Crit Care Med* 27: 2792–2798, 1999.

19. Johnson W, Omland T, Hall C, Lucas C, Myking OL, Collins C, Pfeffer M, Rouleau JL, and Stevenson LW. Neurohormonal activation rapidly decreases after intravenous therapy with diuretics and vasodilators for class IV heart failure. *J Am Coll Cardiol* 39: 1623–1629, 2002.

20. Kaplan JA and Guffin AV. Treatment of perioperative left ventricular failure. In: *Cardiac Anesthesia* (3rd ed.), edited by Kaplan JA. Philadelphia, PA: Saunders, 1993, p. 1058–1094.

21. Martin C, Viviand X, Arnaud S, Vialet R, and Rougnon T. Effects of norepinephrine plus dobutamine or norepinephrine alone on left ventricular performance of septic shock patients. *Crit Care Med* 27: 1708–1713, 1999.

22. Ogilvie RI and Zborowska-Sluis D. Effects of nitroglycerin and nitroprusside on vascular capacitance of anesthetized ganglion-blocked dogs. *J Cardiovasc Pharmacol* 18: 574–580, 1991.

23. Pouleur H, Covell JW, and Ross J Jr. Effects of nitroprusside on venous return and central blood volume in the absence and presence of acute heart failure. *Circulation* 61: 328–337, 1980.

24. Uemura K, Kawada T, Kamiya A, Aiba T, Hidaka I, Sunagawa K, and Sugimachi M. Prediction of circulatory equilibrium in response to changes in stressed blood volume. *Am J Physiol Heart Circ Physiol* 289: H301–H307, 2005.

25. Uemura K, Sugimachi M, Kawada T, Kamiya A, Jin Y, Kashihara K, and Sunagawa K. A novel framework of circulatory equilibrium. *Am J Physiol Heart Circ Physiol* 286: H2376–H2385, 2004.

26. Voss GI, Katona PG, and Chizeck HJ. Adaptive multivariable drug delivery: control of arterial pressure and cardiac output in anesthetized dogs. *IEEE Trans Biomed Eng* 34: 617–623, 1987.

27. Yu C, Roy RJ, Kaufman H, and Bequette BW. Multiple-model adaptive predictive control of mean arterial pressure and cardiac output. *IEEE Trans Biomed Eng* 39: 765–778, 1992.